

Excitation function of initial temperature of heavy flavor quarkonium emission source in high energy collisions

Qi Wang^{1,2,*}, Fu-Hu Liu^{1,2,†}

¹*Institute of Theoretical Physics & State Key Laboratory of Quantum Optics and Quantum Optics Devices, Shanxi University, Taiyuan, Shanxi 030006, People's Republic of China*

²*Collaborative Innovation Center of Extreme Optics, Shanxi University, Taiyuan, Shanxi 030006, People's Republic of China*

Abstract: The transverse momentum spectra of J/ψ , $\psi(2S)$, and $\Upsilon(nS, n = 1, 2, 3)$ produced in proton-proton ($p+p$), proton-antiproton ($p+\bar{p}$), proton-lead ($p+Pb$), gold-gold ($Au+Au$), and lead-lead ($Pb+Pb$) collisions over a wide energy range are analyzed by the (two-component) Erlang distribution, the Hagedorn function (the inverse power-law), and the Tsallis-Levy function. The initial temperature is obtained from the color string percolation model from the fit by the (two-component) Erlang distribution in the framework of multisource thermal model. The excitation functions of several parameters such as the mean transverse momentum and initial temperature increase from 39 GeV to 13 TeV which is considered in this work. The mean transverse momentum and initial temperature decrease (increase slightly or do not change significantly) with the increase of rapidity (centrality). Meanwhile, the mean transverse momentum of $\Upsilon(nS, n = 1, 2, 3)$ is larger than that of J/ψ and $\psi(2S)$, and the initial temperature for $\Upsilon(nS, n = 1, 2, 3)$ emission is higher than that for J/ψ and $\psi(2S)$ emission, which shows a mass-dependent behavior.

Keywords: Excitation function, mean transverse momentum, initial state temperature, (two-component) Erlang distribution

PACS: 12.40.Ee, 14.20.-c, 24.10.Pa, 25.75.Ag

1 Introduction

The excitation functions of some physical quantities are significative to help us to understand the nuclear reaction mechanism and the system evolution characteristic. For instance, the higher the mean transverse momentum ($\langle p_T \rangle$) is, the higher excitation state the emission source stays at. Meanwhile, the higher the initial temperature (T_i) [1, 2, 3, 4, 5] is, the more violent the collisions are. By the analysis of the excitation functions of $\langle p_T \rangle$ and T_i , we can learn more about the process in high energy collisions in which the excitation functions of several parameters such as $\langle p_T \rangle$ and T_i can be obtained from the p_T spectra of produced particles.

In a data-driven reanalysis, to obtain $\langle p_T \rangle$ and T_i , at the first place, we need the p_T spectra of particles in experiments. At the second place, we should choose appropriate functions such as the Erlang distribution [6, 7, 8], the Hagedorn function or the inverse power-law [9, 10], the Tsallis-Levy function [11, 12], and others. At the last place, we use the chosen functions to fit the expe-

riential data on particle spectra. By describing the p_T spectra, the parameters from the selected functions can be extracted. By comparing the parameters obtained from the experiential data at different energies, centralities, and rapidities, we can find out the dependences of parameters on these quantities. These dependences are related to excitation and expansion degrees of emission source, which is beneficial for us to understand the mechanism and characteristic of nuclear reactions and system evolution.

Besides the two derived parameters $\langle p_T \rangle$ and T_i , we can obtain other related parameters by using the method which is similar to extract $\langle p_T \rangle$ and T_i . For example, using the Hagedorn function or the inverse power-law [9, 10] and the Tsallis-Levy function [11, 12] to fit p_T spectra, some free parameters such as p_0 , n_0 , T , and n in the mentioned functions which will be discussed in section 2 can be extracted. These free parameters are also useful to understand particle productions and system evolution. Not only the excitation functions

*E-mail: 18303476022@163.com or qiwang-sxu@qq.com

†Correspondence E-mail: fuhuliu@163.com or fuhuliu@sxu.edu.cn

of derived parameters $\langle p_T \rangle$ and T_i but also the trends of free parameters p_0 , n_0 , T , and n can be studied from the fit to p_T spectra.

In this work, the (two-component) Erlang distribution [6, 7, 8], Hagedorn function (the inverse power-law) [9, 10], and Tsallis-Levy function [11, 12] are introduced firstly in section 2. Then, in section 3, the three distributions or functions are used to preliminarily fit the p_T spectra of heavy flavor quarkonia (charmonia and bottomonia) produced in high energy collisions. The function results are compared with the spectra of J/ψ , $\psi(2S)$, and $\Upsilon(nS, n = 1, 2, 3)$ measured by the STAR [13, 14], CDF [15, 16, 17], ALICE [18], LHCb [19, 20, 21, 22, 23, 24, 25, 26, 27], ATLAS [28, 29, 30], and CMS Collaborations [31, 32, 33, 34] over a wide energy range. Finally, in section 4, we give our summary and conclusions.

2 Formalism and method

2.1 The (two-component) Erlang distribution

According to the multisource thermal model [6, 7, 8], a given particle is produced in the collision process where a few partons or quarks have taken part in. Each (the i -th) parton is assumed to contribute to an exponential function [$f_i(p_t)$] of transverse momentum (p_t) distribution. Let $\langle p_t \rangle$ denotes the mean transverse momentum contributed by the i -th parton, we have the probability density function of p_t to be

$$f_i(p_t) = \frac{1}{\langle p_t \rangle} \exp \left(-\frac{p_t}{\langle p_t \rangle} \right) \quad (1)$$

which is normalized to 1. The probability density function of p_T contributed by all N partons which have taken part in the collision process is the convolution of N exponential functions [6, 7, 8]. We have the p_T distribution $f_E(p_T)$ (the probability density function of p_T) of final state particles to be the Erlang distribution

$$f_E(p_T) = \frac{p_T^{N-1}}{(N-1)! \langle p_t \rangle^N} \exp \left(-\frac{p_T}{\langle p_t \rangle} \right) \quad (2)$$

which is naturally normalized to 1. The mean p_T is $\langle p_T \rangle = N \langle p_t \rangle$.

In the two-component Erlang distribution, we have

$$\begin{aligned} f_1(p_T) &= \frac{k_E p_T^{N_1-1}}{(N_1-1)! \langle p_t \rangle_1^{N_1}} \exp \left(-\frac{p_T}{\langle p_t \rangle_1} \right) \\ &+ \frac{(1-k_E)p_T^{N_2-1}}{(N_2-1)! \langle p_t \rangle_2^{N_2}} \exp \left(-\frac{p_T}{\langle p_t \rangle_2} \right), \end{aligned} \quad (3)$$

where k_E denotes the contribution fraction of the first component, N_1 (N_2) denotes the number of partons in the first (second) component, and $\langle p_t \rangle_1$ ($\langle p_t \rangle_2$) denotes the mean transverse momentum contributed by each parton in the first (second) component. The mean p_T is $\langle p_T \rangle = k_E N_1 \langle p_t \rangle_1 + (1-k_E) N_2 \langle p_t \rangle_2$, where $N_1 = 1-3$ in this work and $N_2 = 2$ if $1-k_E \neq 0$.

2.2 The (two-component) Hagedorn function

The Hagedorn function is an inverse power-law which is suitable to describe wide p_T spectra of particles produced in hard scattering process. In refs. [9, 10], the Hagedorn function or the inverse power-law shows the probability density function of p_T to be

$$f_H(p_T) = A p_T \left(1 + \frac{p_T}{p_0} \right)^{-n_0}, \quad (4)$$

where p_0 and n_0 are the free parameters and A is the normalization constant which is related to p_0 and n_0 and results in $\int_0^\infty f_H(p_T) dp_T = 1$. Eq. (6) is an empirical formula inspired by quantum chromodynamics (QCD). We call Eq. (4) the Hagedorn function or the inverse power-law [9, 10].

In the case of using two-component Hagedorn function, we have

$$\begin{aligned} f_2(p_T) &= k_H A_1 p_T \left(1 + \frac{p_T}{p_{01}} \right)^{-n_{01}} \\ &+ (1-k_H) A_2 p_T \left(1 + \frac{p_T}{p_{02}} \right)^{-n_{02}}, \end{aligned} \quad (5)$$

where k_H denotes the contribution fraction of the first component, A_1 (A_2) is the normalization constant which results in the first (second) component to be normalized to 1, and p_{01} (p_{02}) and n_{01} (n_{02}) are free parameters related to the first (second) component. To combine the free parameters of the two components, we have $p_0 = k_H p_{01} + (1-k_H) p_{02}$ and $n_0 = k_H n_{01} + (1-k_H) n_{02}$.

Generally, Eq. (4) is possible to describe the spectra in both the low- and high- p_T regions. In fact, the spectra in the low- and high- p_T regions represent similar trend in some cases. This is caused due to the similarity [35, 36, 37, 38, 39, 40, 41, 42, 43, 44, 45] which is widely existent in high energy collisions, where the similarity means the common or universality laws existed in different processes or collisions. In addition, one can revise Eq. (4) if needed in different ways [46, 47, 48, 49, 50, 51, 52] which suppress in the spectrum itself in low- or high- p_T region according to the experimental spectra. To discuss various revisions of the Hagedorn function or the inverse power-law [9, 10]

is beyond the focus of this paper. We shall not discuss anymore on this issue. For a very wide p_T spectrum, Eq. (5) is possibly needed.

2.3 The (two-component) Tsallis-Levy function

The Tsallis statistics [11] has wide applications in high energy collisions. There are various forms of the Tsallis distribution or function. In this work, we use the Tsallis-Levy function [12]

$$f_L(p_T) = C p_T \left(1 + \frac{\sqrt{p_T^2 + m_0^2} - m_0}{nT} \right)^{-n}, \quad (6)$$

where T and n are free parameters, $\sqrt{p_T^2 + m_0^2} \equiv m_T$ is the transverse mass, m_0 is the rest mass of the considered particle, and C is the normalized constant which is related to T , n , and m_0 and results in $\int_0^\infty f_L(p_T) dp_T = 1$.

We notice that $f_L(p_T)$ is related to particle mass m_0 , which is not the case of $f_E(p_T)$ and $f_H(p_T)$ presented in Eqs. (2) and (4) respectively. Although $f_L(p_T)$ is related to m_0 , this relation is not strong due to m_0 appearing only in $\sqrt{p_T^2 + m_0^2} - m_0$. The fact that the Tsallis distribution depends on m_0 shows that this takes simple kinematics into account, as it is well known that m_T or $m_T - m_0$ (something like transverse kinetic energy) is a better “scaling variable” for the spectra than p_T .

In the case of using two-component Tsallis-Levy function, we have

$$f_3(p_T) = k_L C_1 p_T \left(1 + \frac{\sqrt{p_T^2 + m_0^2} - m_0}{n_1 T_1} \right)^{-n_1} + (1 - k_L) C_2 p_T \left(1 + \frac{\sqrt{p_T^2 + m_0^2} - m_0}{n_2 T_2} \right)^{-n_2}, \quad (7)$$

where k_L denotes the contribution fraction of the first component, C_1 (C_2) is the normalization constant which results in the first (second) component to be normalized to 1, and T_1 (T_2) and n_1 (n_2) are free parameters. To combine the free parameters of the two components, we have $T = k_L T_1 + (1 - k_L) T_2$ and $n = k_L n_1 + (1 - k_L) n_2$.

The temperature parameter in the Tsallis-Levy function is an effective temperature at the final state (the stage of kinetic freeze-out). This effective temperature is not a “real” temperature because it includes not only the contribution of random thermal motion but also the contribution of flow effect. In the case of the first (second) component having T_1 (T_2) with the fraction of k_L ($1 - k_L$), the common effective temperature T of the two components is extracted from the assumed

common equilibrium state of the two components. That is $T = k_L T_1 + (1 - k_L) T_2$ which has the same form as the parameter n .

2.4 The initial temperature

According to the color string percolation model [53, 54, 55], the initial temperature of the emission source is determined by

$$T_i \equiv \sqrt{\frac{\langle p_T^2 \rangle}{2}} \quad (8)$$

where

$$\langle p_T^2 \rangle = \int_0^\infty p_T^2 f_{1,2,3}(p_T) dp_T \quad (9)$$

is the square of the root-mean-square of p_T due to $\int_0^\infty f_{1,2,3}(p_T) dp_T = 1$. If the x -component (p_x) and y -component (p_y) of the transverse momentum p_T are considered, we have

$$T_i = \sqrt{\langle p_x^2 \rangle} = \sqrt{\langle p_y^2 \rangle}. \quad (10)$$

In the source rest-frame and under the assumption of isotropic emission, if the z -component of momentum is p'_z , we also have

$$T_i = \sqrt{\langle p_z'^2 \rangle}. \quad (11)$$

Although the source rest-frame is the lab-frame for symmetric collisions, we have mentioned the source rest-frame because asymmetric proton-lead (p +Pb) collisions are also considered in this work.

It should be noted that we have used a single string in the cluster for a given particle production because only a projectile participant quark and a target participant quark are mainly considered in our treatment. The assumption of the single string results in the color suppression factor $F(\xi)$ to be 1 in the color string percolation model [54]. If we consider more than one strings taking part in the given particle production, the minimum $F(\xi)$ will be nearly 0.6 [54]. Thus, we shall obtain a higher T_i by multiplying a revised factor $1/\sqrt{F(\xi)}$ in Eqs. (8), (10), and (11). In our opinion, although more than one strings have influences on the given particle production, the main role is the single string.

2.5 Discussion on the functions

We would like to point out that the three types of functions are mainly just used here as parametrizations to achieve a good fit to the data, to be able to extract $\langle p_T \rangle$ and T_i , though the Hagedorn and Tsallis-Levy functions are physically relevant. In fact, in the two functions, if we let $m_0 = 0$, $p_0 = nT$, $n_0 = n = 1/(q-1)$,

the two functions are the same. Here q is an entropy index that characterizes the excitation degree of the collision system [11, 12]. Generally, n_0 or n is a sizeable quantity, which results in q to close to 1 and the collision system to close to an equilibrium state.

We have used the two-component functions in some cases. The reason for using two-component source, i.e. basically two temperatures is not just used to achieve a better fit to the data. Physically, the first component corresponds to the non-head-on collisions between projectile and target participant quarks. The second component corresponds to the head-on collisions between the two quarks. Generally, the first component has a large fraction and low $\langle p_T \rangle$ and T_i . The second component has a less fraction and high $\langle p_T \rangle$ and T_i . Because the head-on collisions between the two quarks are infrequent, single component function is usually applicable.

In principal, no matter what functions are used to fit the experimental data, $\langle p_T \rangle$ (or T_i) obtained from different fits are approximately the same within a small systematic uncertainty, if different functions fit the data good enough in the p_T region of data available. For example, if simple Maxwell-Boltzmann or Bose-Einstein statistics can fit the data, we may obtain similar $\langle p_T \rangle$ (or T_i) with other functions. In the case of multi-component Maxwell-Boltzmann or Bose-Einstein statistics being needed, we may also obtain similar $\langle p_T \rangle$ (or T_i).

Indeed, the data itself decides $\langle p_T \rangle$ (or T_i), and $\langle p_T \rangle$ (or T_i) can be directly obtained from the data itself. The reason why we use functions is to see the tendency where the data is not available. However, the extrapolation on the tendency should be careful because it is not fully true, as it to the low- and high p_T regions (where there is no data) could in principle have a major effect on the tendency (for example in case of very step exponentials near $p_T = 0$, or power-law tails at large p_T). To reduce the effect, the data should be measured in a sufficiently large p_T interval so that the extrapolation does not spoil as far as possible.

For different components and functions, we do not need to consider the values of mid-rapidity (mid- y) or mid-pseudorapidity (mid- η), or the values of mid- y or mid- η can be regarded as 0 directly. In fact, for the experimental data with non-zero mid- y or mid- η , we may directly regard them as those with mid- $y = 0$ or mid- $\eta = 0$. This treatment is performed to subtract the contribution of kinetic energy of directed motion to the temperature.

3 Results and discussion

Ordered by center-of-mass energy per nucleon pair ($\sqrt{s_{NN}}$ or \sqrt{s} if only one pair) for different panels, Fig. 1 shows the p_T spectra, (a)–(c) $(1/2\pi p_T)d^2N/dp_T dy$, (d)–(e) $(1/2\pi p_T)d^2\sigma/dp_T dy$, (f) $d^2\sigma/dp_T dy$, and (g) $d^2Y/dp_T dy$, of (a)–(d) $J/\psi \rightarrow e^+e^-$, (e) $J/\psi \rightarrow \mu^+\mu^-$, (f) prompt J/ψ , and (g) inclusive J/ψ produced in (a)–(c) gold-gold (Au+Au), (d)–(e) proton-proton ($p+p$), (f) proton-antiproton ($p+\bar{p}$), and (g) lead-lead (Pb+Pb) collisions at mid-rapidity (a)–(d) $|y| < 1$, (e) $|y| < 0.4$, (f) $|y| < 0.6$, and forward rapidity (g) $2.5 < y < 4$ at $\sqrt{s_{NN}}$ or $\sqrt{s} =$ (a) 39, (b) 62.4, (c) 200, (d) 500, and (e) 510 GeV, as well as (f) 1.8 and 1.96, and (g) 2.76 TeV, where N denotes the number of particles, σ denotes the cross section, and Y denotes the yield. The symbols represent the experimental data [13, 14, 15, 16, 18] and the curve are our fitted results. In the calculations, the method of least square is used to obtain the best free parameters. The values of free parameters $\langle p_t \rangle_1$, $\langle p_t \rangle_2$, N_1 , and k_E are listed in Table A1 with χ^2 and number of degree of freedom (ndof) in the appendix 1. The values of free parameters p_0 , n_0 , T , and n are listed in Table A2 with χ^2 and ndof in the appendix. One can see that the (two-component) Erlang distribution, the Hagedorn function, and the Tsallis-Levy function fit approximately the experimental p_T spectra of J/ψ via different decay or production modes in high energy $p+p$, $p+\bar{p}$, Au+Au, and Pb+Pb collisions.

The p_T spectra, $d^2\sigma/dp_T dy$, of (a)(c)(e)(g) prompt J/ψ and (b)(d)(f)(h) J/ψ from b produced in (a)(b) $p+Pb$ and (c)–(h) $p+p$ collisions at $\sqrt{s_{NN}}$ or $\sqrt{s} =$ (a)(b) 5, (c)(d) 7, (e)(f) 8, and (g)(h) 13 TeV are presented in Fig. 2. The symbols represent the experimental data [19, 20, 21, 22] and the curve are our fitted results. The method of least square is used to obtain the best parameter values which are listed in Tables A1 and A2 with χ^2 and ndof. One can see that the experimental p_T spectra of J/ψ via different production modes in different rapidity intervals in $p+p$ and $p+Pb$ collisions at high energies are approximately fitted by the Erlang distribution, the Hagedorn function, and the Tsallis-Levy function.

Figure 3 shows the p_T spectra, (a)(c)–(g) $d^2\sigma/dp_T dy$ and (b) $d\sigma/dp_T$, of $\psi(2S)$ via different production modes. The symbols represent the experimental data [15, 16, 23, 28, 31, 32] and the curve are our fitted results. The values of free parameters are listed in Tables A1 and A2 with χ^2 and ndof. One can see that the experimental p_T spectra of $\psi(2S)$ via different produc-

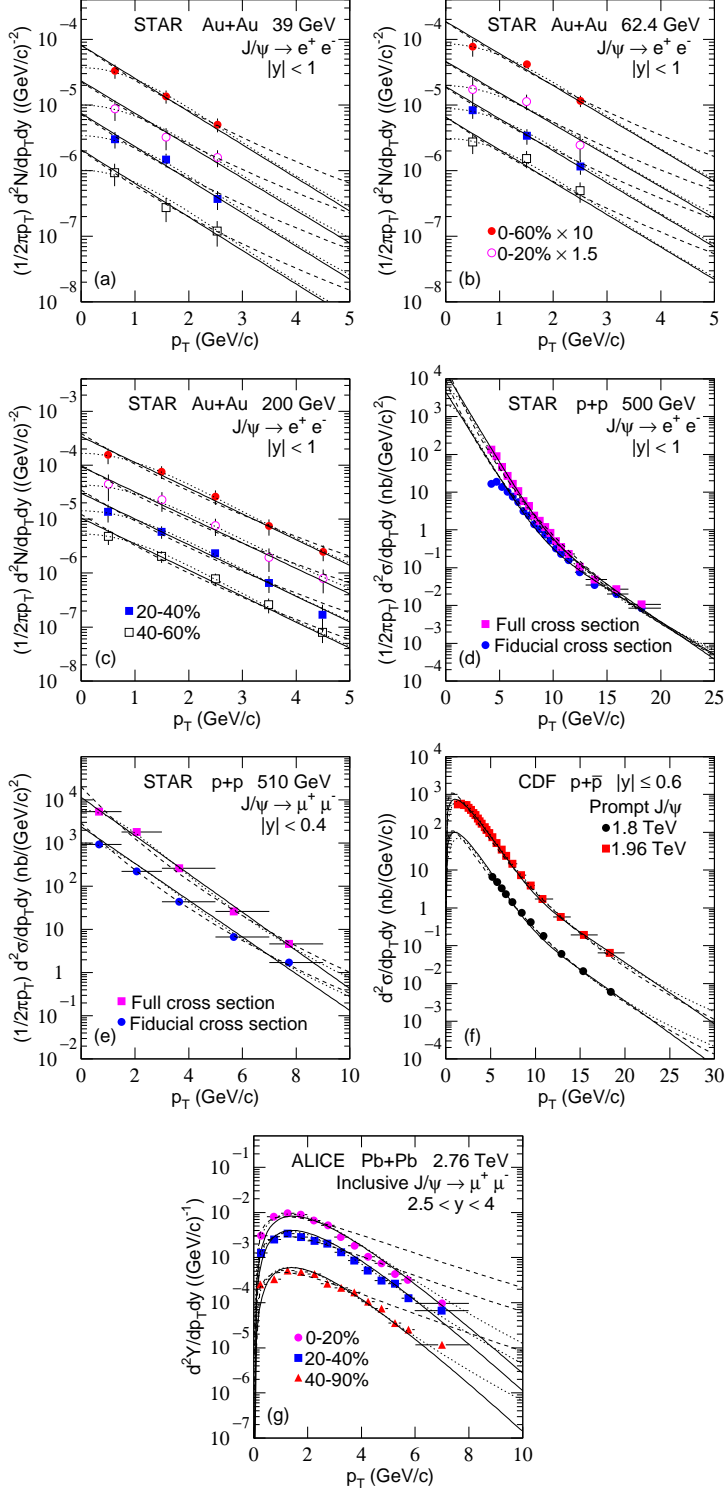


Fig. 1. Transverse momentum spectra, (a)–(c) $(1/2\pi p_T)d^2N/dp_T dy$, (d)(e) $(1/2\pi p_T)d^2\sigma/dp_T dy$, (f) $d^2\sigma/dp_T dy$, and (g) $d^2Y/dp_T dy$ of J/ψ in different decay or production modes in (a)–(c) Au+Au, (d)(e) $p+p$, (f) $p+\bar{p}$, and (g) Pb+Pb collisions at energies (a) 39, (b) 62.4, (c) 200, (d) 500, and (e) 510 GeV, as well as (f) 1.8 and 1.96, and (g) 2.76 TeV. The experimental data represented by the symbols are measured by the (a)–(e) STAR [13, 14], (f) CDF [15, 16], and (g) ALICE Collaborations [18] with different centrality classes such as (a)–(c) 0-20%, 20-40%, 40-60%, and 0-60%, and (g) 0-20%, 20-40%, and 40-90%, as well as with different cross sections e.g. (d)(e) full and fiducial cross sections. Some data points are scaled by different amounts marked in the panels. The data points are fitted by the (two-component) Erlang distribution (Eq. (3), the solid curve), the Hagedorn function (Eq. (4), the dashed curve), and the Tsallis-Levy function (Eq. (6), the dotted curve), respectively.

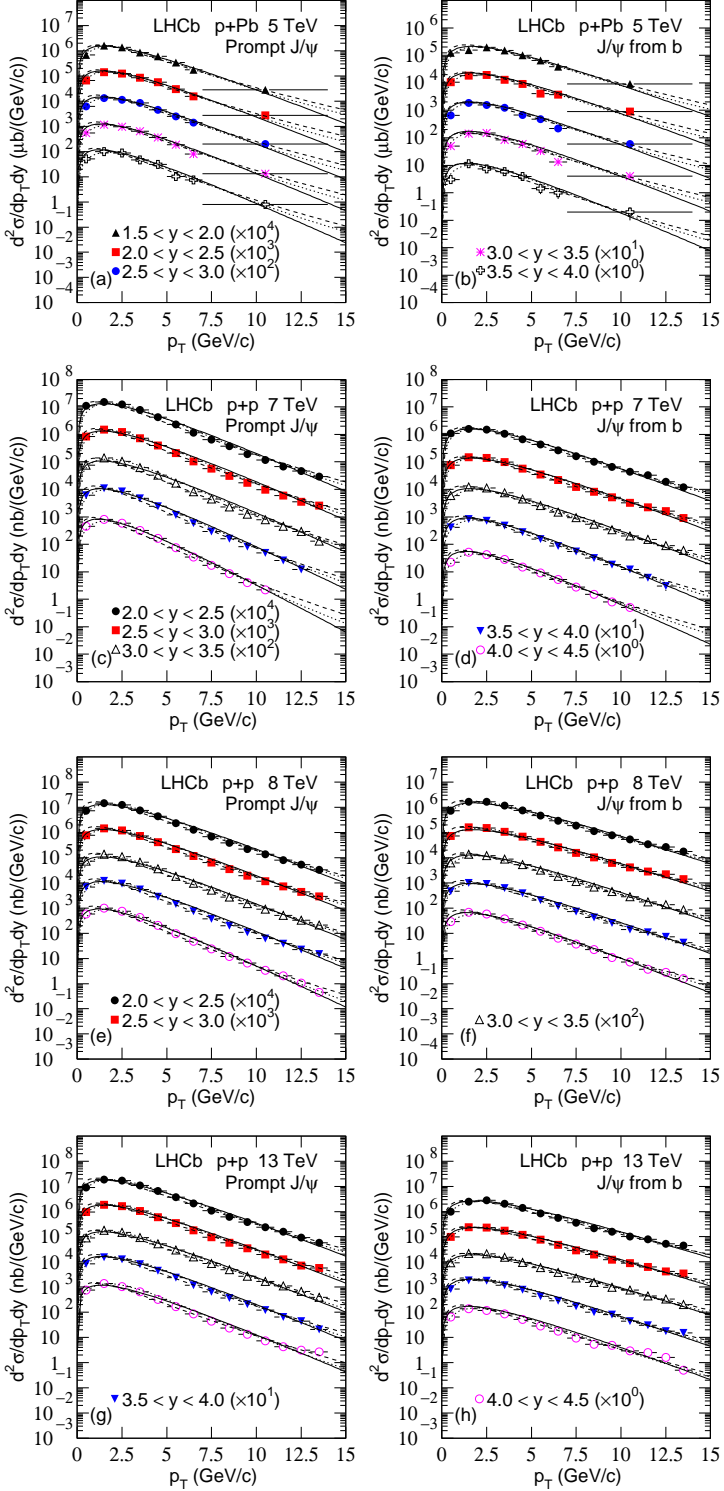


Fig. 2. Transverse momentum spectra, $d^2\sigma/dp_T dy$, of J/ψ in different production modes in (a)(b) $p+Pb$ and (c)–(h) $p+p$ collisions at (a)(b) 5, (c)(d) 7, (e)(f) 8, and (g)(h) 13 TeV. The different symbols represent the experimental data measured by the LHCb Collaboration [19, 20, 21, 22] in the rapidity intervals of (a)(b) $1.5 < y < 2.0$, $2.0 < y < 2.5$, $2.5 < y < 3.0$, $3.0 < y < 3.5$, and $3.5 < y < 4.0$ and (c)–(h) $2.0 < y < 2.5$, $2.5 < y < 3.0$, $3.0 < y < 3.5$, $3.5 < y < 4.0$, and $4.0 < y < 4.5$, and scaled by different amounts marked in the panels. The solid, dashed, and dotted curves represent our results fitted by the Erlang distribution (Eq. (3)), the Hagedorn function (Eq. (4)), and the Tsallis-Levy function (Eq. (6)), respectively.

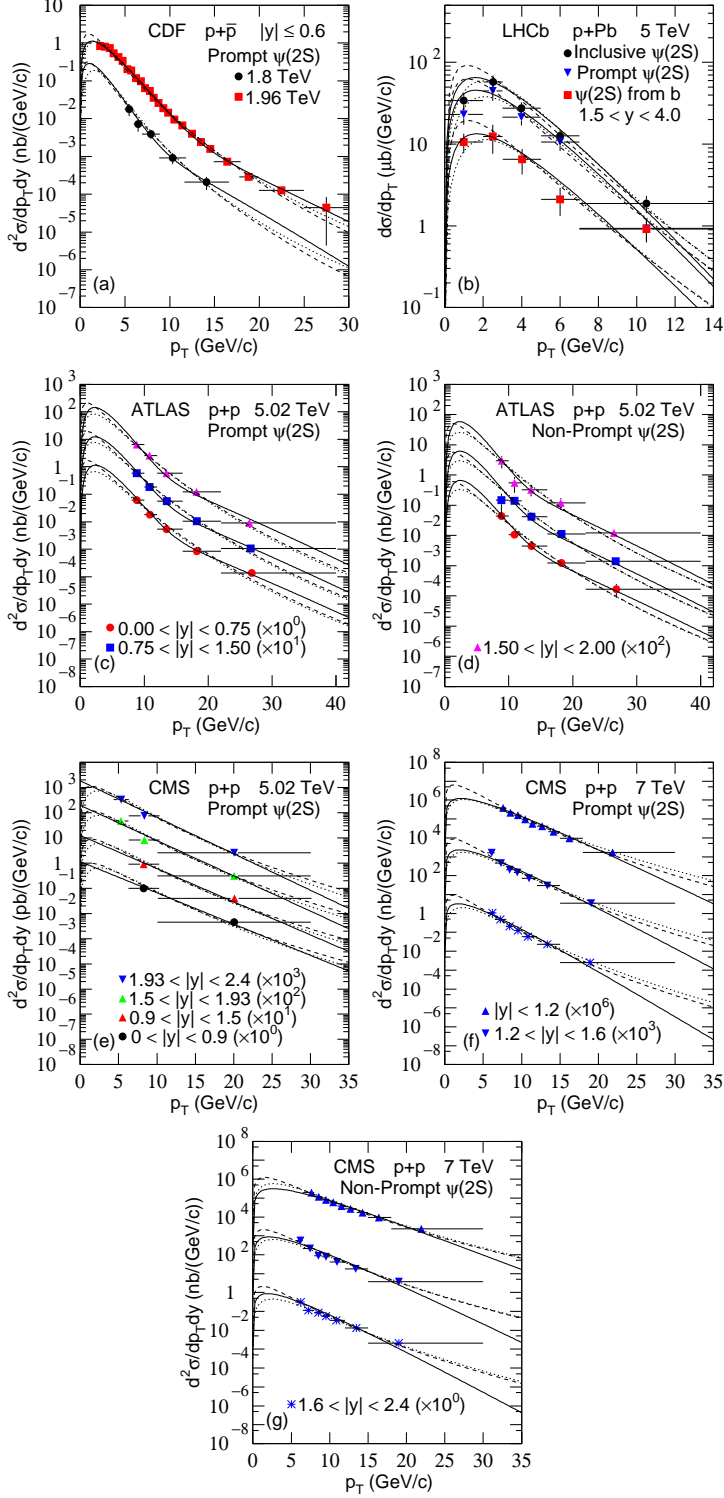


Fig. 3. Transverse momentum spectra, (a)(c)–(g) $d^2\sigma/dp_T dy$ and (b) $d\sigma/dp_T$, of $\psi(2S)$ from different production modes in (a) $p+\bar{p}$, (b) $p+Pb$, and (c)–(g) $p+p$ collisions at energies (a) 1.8 and 1.96, (b) 5, (c)–(e) 5.02, and (f)–(g) 7 TeV. The different symbols represent the experimental data of the (a)(c)(e)(f) prompt $\psi(2S)$, (b) inclusive $\psi(2S)$, prompt $\psi(2S)$, and $\psi(2S)$ from b , and (d)(g) non-prompt $\psi(2S)$ measured by the (a) CDF [15, 16], (b) LHCb [23], (c)(d) ATLAS [28], and (e)–(g) CMS Collaborations [31, 32] in (a) $p+\bar{p}$, (b) $p+Pb$, (c)–(g) $p+p$ collisions at $\sqrt{s_{NN}}$ or $\sqrt{s} =$ (a) 1.8 and 1.96, (b) 5, (c)–(e) 5.02, and (f)(g) 7 TeV with (a) $|y| < 0.6$, (b) $1.5 < y < 4.0$, (c)(d) $0.00 < |y| < 0.75$, $0.75 < |y| < 1.50$, and $1.50 < |y| < 2.00$, (e) $0 < |y| < 0.9$, $0.9 < |y| < 1.5$, $1.5 < |y| < 1.93$, and $1.93 < |y| < 2.4$, and (f)(g) $|y| < 1.2$, $1.2 < |y| < 1.6$, and $1.6 < |y| < 2.4$, where different collaborations have used different precisions for the rapidity intervals. Some data points are scaled by different amounts marked in the panels. The solid, dashed, and dotted curves represent our results fitted by the (two-component) Erlang distribution (Eq. (3)), the Hagedorn function (Eq. (4)), and the Tsallis-Levy function (Eq. (6)), respectively.

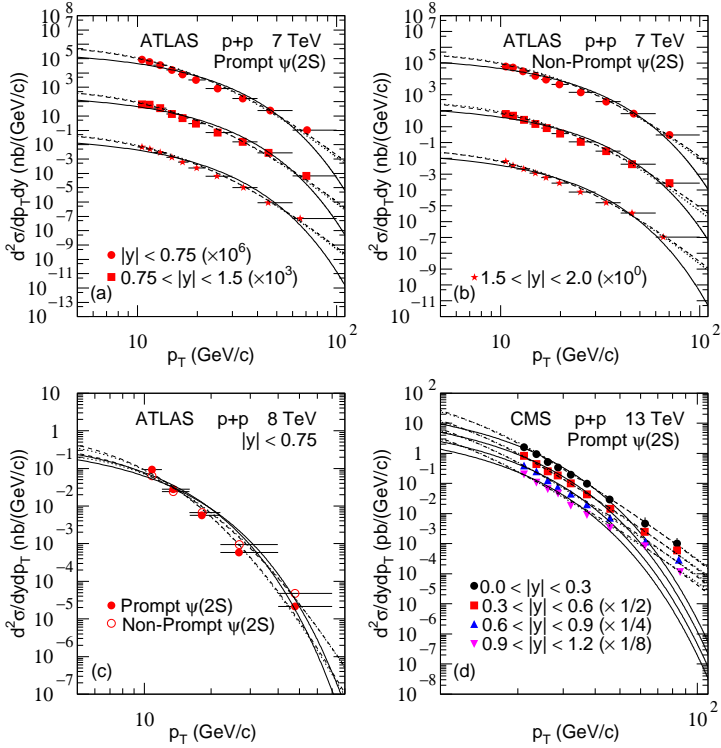


Fig. 4. Same as Fig. 3, but showing the results at (a)(b) 7, (c) 8, and (d) 13 TeV. The different symbols represent the experimental data of (a)(d) prompt $\psi(2S)$, (b) non-prompt $\psi(2S)$, and (c) prompt $\psi(2S)$ and non-prompt $\psi(2S)$ measured by the (a)–(c) ATLAS [29, 30] and (d) CMS Collaborations [33] in (a)(b) $|y| < 0.75$, $0.75 < |y| < 1.5$, and $1.5 < |y| < 2.0$, (c) $|y| < 0.75$, and (d) $0.0 < |y| < 0.3$, $0.3 < |y| < 0.6$, $0.6 < |y| < 0.9$, and $0.9 < |y| < 1.2$, where some data points are scaled by different amounts marked in the panels. The data points are fitted by the Erlang distribution (Eq. (3), the solid curve), the Hagedorn function (Eq. (4), the dashed curves), and the Tsallis-Levy function (Eq. (6), the dotted curves). In particular, the two-component Hagedorn function (Eq. (5), the dashed curves) and the two-component Tsallis-Levy function (Eq. (7), the dotted curves) are used in Fig. 4(d).

tion modes in different rapidity intervals in $p+p$, $p+\bar{p}$, and $p+Pb$ collisions at high energies are approximately fitted by the (two-component) Erlang distribution, the Hagedorn function, and the Tsallis-Levy function.

Figure 4 shows the p_T spectra, $d^2\sigma/dp_T dy$, of $\psi(2S)$ via different production modes in $p+p$ collisions at $\sqrt{s} =$ (a)(b) 7, (c) 8, and (d) 13 TeV. The symbols represent the experimental data [29, 30, 33] and the curve are our fitted results. The values of free parameters are listed in Tables A1 and A2 with χ^2 and ndof. For Fig. 4(d), the two-component Eqs. (5) and (7) are used, where the free parameters for the first (second) component are listed in the first (second) row. One can see that the experimental p_T spectra of $\psi(2S)$ via different production modes in different rapidity intervals in $p+p$ collisions at high energies are also approximately fitted by the Erlang distribution, the (two-component) Hagedorn function, and the (two-component) Tsallis-Levy function.

In Fig. 5, the p_T spectra, (a)(c)–(f) $d^2\sigma/dp_T dy$ and

(b) $d\sigma/dp_T$, of (a)–(c) $\Upsilon(nS, n = 1, 2, 3) \rightarrow \mu^+\mu^-$, (d) $\Upsilon(1S) \rightarrow \mu^+\mu^-$, (e) $\Upsilon(2S) \rightarrow \mu^+\mu^-$, and (f) $\Upsilon(3S) \rightarrow \mu^+\mu^-$ induced in (a) $p+\bar{p}$ and (b)–(f) $p+p$ collisions at $\sqrt{s} =$ (a) 1.8, (b) 2.76, (c) 5.02, and (d)–(f) 7 TeV are given. The symbols represent the experimental data [17, 24, 25, 34] and the curve are our fitted results. The parameter values are listed in Tables A1 and A2 with χ^2 and ndof. One can see that the experimental p_T spectra of $\Upsilon(nS, n = 1, 2, 3) \rightarrow \mu^+\mu^-$ in different rapidity intervals in $p+p$ and $p+\bar{p}$ collisions at high energies are approximately fitted by the Erlang distribution, the Hagedorn function, and the Tsallis-Levy function.

In Fig. 6, the p_T spectra, $d^2\sigma/dp_T dy$, of (a)(d)(e) $\Upsilon(1S) \rightarrow \mu^+\mu^-$, (b)(f) $\Upsilon(2S) \rightarrow \mu^+\mu^-$, and (c)(g) $\Upsilon(3S) \rightarrow \mu^+\mu^-$ induced in (a)–(c) and (e)–(g) $p+p$ and (d) $p+Pb$ collisions at $\sqrt{s_{NN}}$ or $\sqrt{s} =$ (a)–(c) 8, (d) 8.16, and (e)–(g) 13 TeV are given. The symbols represent the experimental data [25, 26, 27] and the curve are our

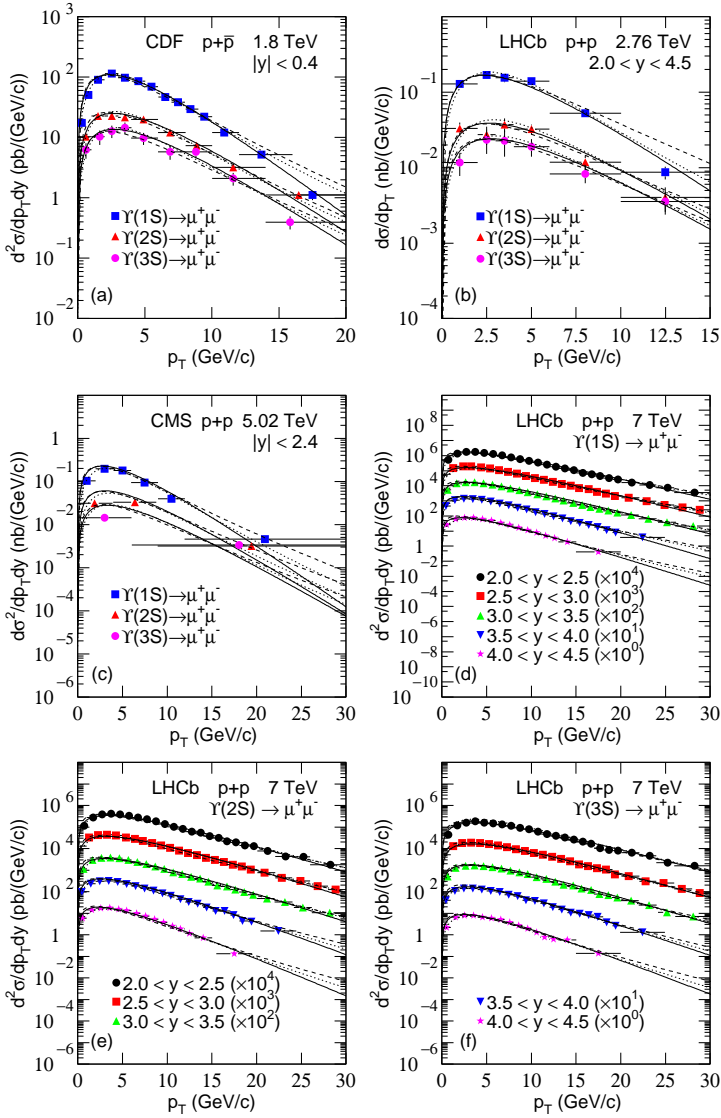


Fig. 5. Transverse momentum spectra, (a)(c)–(f) $d^2\sigma/dp_T dy$ and (b) $d\sigma/dp_T$, of (a)–(c) $\Upsilon(nS, n = 1, 2, 3) \rightarrow \mu^+\mu^-$, (d) $\Upsilon(1S) \rightarrow \mu^+\mu^-$, (e) $\Upsilon(2S) \rightarrow \mu^+\mu^-$, and (f) $\Upsilon(3S) \rightarrow \mu^+\mu^-$ in (a) $p+\bar{p}$ and (b)–(f) $p+p$ collisions at (a) 1.8, (b) 2.76, (c) 5.02, and (d)–(f) 7 TeV. The symbols shown in panels (a)–(c) represent the experimental data measured by the (a) CDF [17], (b) LHCb [24], and (c) CMS Collaborations [34] in (a) $p+\bar{p}$ and (b)(c) $p+p$ collisions in (a) $|y| < 0.4$, (b) $2.0 < y < 4.5$, and (c) $|y| < 2.4$ respectively. The symbols shown in panels (d)–(f) represent the experimental data measured by the LHCb Collaboration [25] in $p+p$ collisions in $2.0 < y < 2.5$, $2.5 < y < 3.0$, $3.0 < y < 3.5$, $3.5 < y < 4.0$, and $4.0 < y < 4.5$ and scaled by different amounts shown in the panels. The data points are fitted by the Erlang distribution (Eq. (3)), the Hagedorn function (Eq. (4)), and the Tsallis-Levy function (Eq. (6)) by the solid, dashed, and dotted curves, respectively.

fitted results. The parameter values are listed in Table A1 and A2 with χ^2 and ndof. Once again, one can see that the experimental p_T spectra of $\Upsilon(nS, n = 1, 2, 3) \rightarrow \mu^+\mu^-$ in different rapidity intervals in $p+p$ and $p+Pb$ collisions at high energies are approximately fitted by the Erlang distribution, the Hagedorn function, and the Tsallis-Levy function.

Before discussing the trends of parameters, we would

like to point out the usability of the concept of temperature in $p+p$ ($p+\bar{p}$) collisions which are small in size. As in refs. [56, 57, 58, 59], in this work, we have treated $p+p$ ($p+\bar{p}$) collisions as where a medium was formed, or at least there is some degree of thermalization, enough to have a temperature for the emission source. On the other hand, the temperature parameter of the emission source is a reflection of average kinetic energy of given

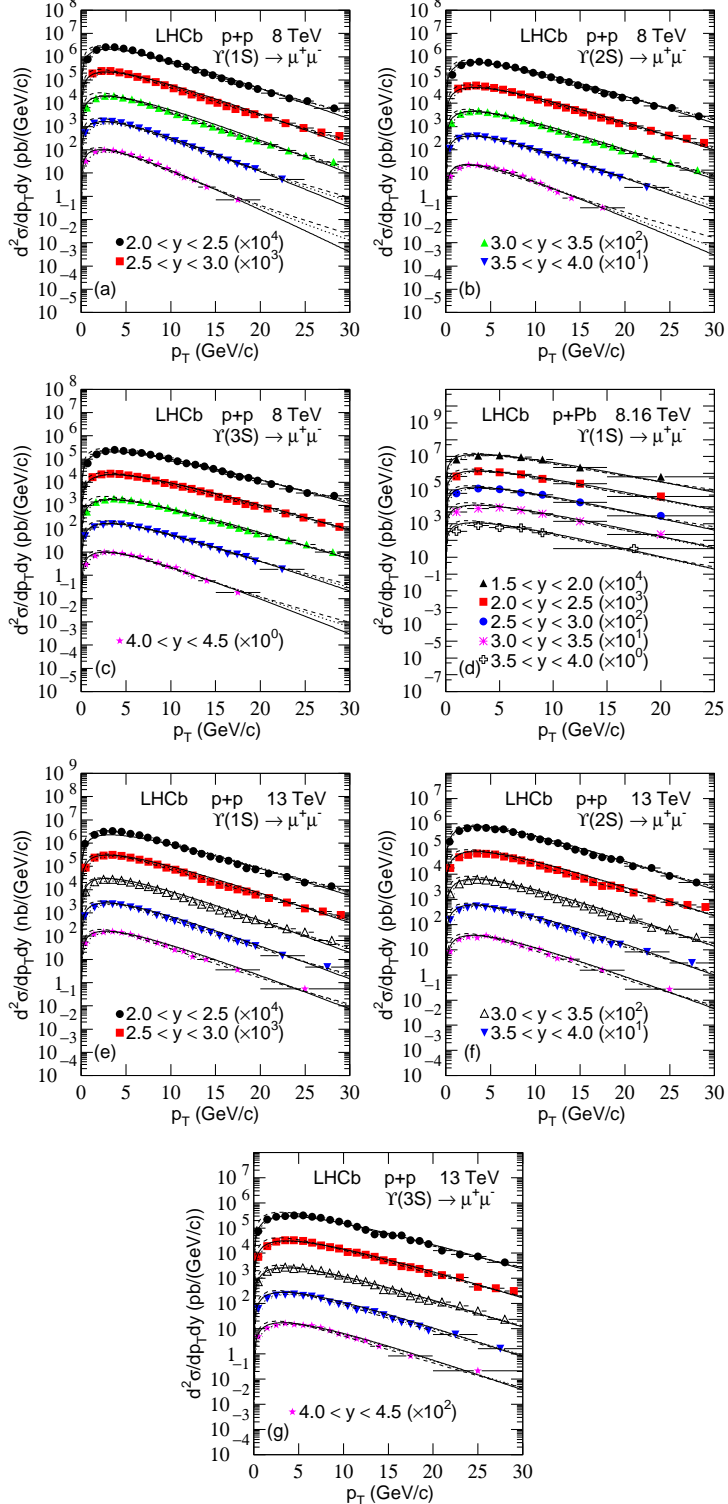


Fig. 6. Transverse momentum spectra, $d^2\sigma/dp_T dy$, of (a)(d)(e) $\Upsilon(1S) \rightarrow \mu^+\mu^-$, (b)(f) $\Upsilon(2S) \rightarrow \mu^+\mu^-$, and (c)(g) $\Upsilon(3S) \rightarrow \mu^+\mu^-$ in (a)–(c) and (e)–(g) $p+p$ and (d) $p+Pb$ collisions at (a)–(c) 8, (d) 8.16, and (e)–(g) 13 TeV. The symbols represent the experimental data measured by the LHCb Collaboration [25, 26, 27]. The rapidity intervals for panels (a)–(c) and (e)–(f) are $2.0 < y < 2.5$, $2.5 < y < 3.0$, $3.0 < y < 3.5$, $3.5 < y < 4.0$, and $4.0 < y < 4.5$. The rapidity intervals for panel (d) are $1.5 < y < 2.0$, $2.0 < y < 2.5$, $2.5 < y < 3.0$, $3.0 < y < 3.5$, and $3.5 < y < 4.0$. Different sets of data points are scaled by different amounts shown in the panels. The data points are fitted by the Erlang distribution (Eq. (3)), the Hagedorn function (Eq. (4)), and the Tsallis-Levy function (Eq. (6)) by the solid, dashed, and dotted curves, respectively.

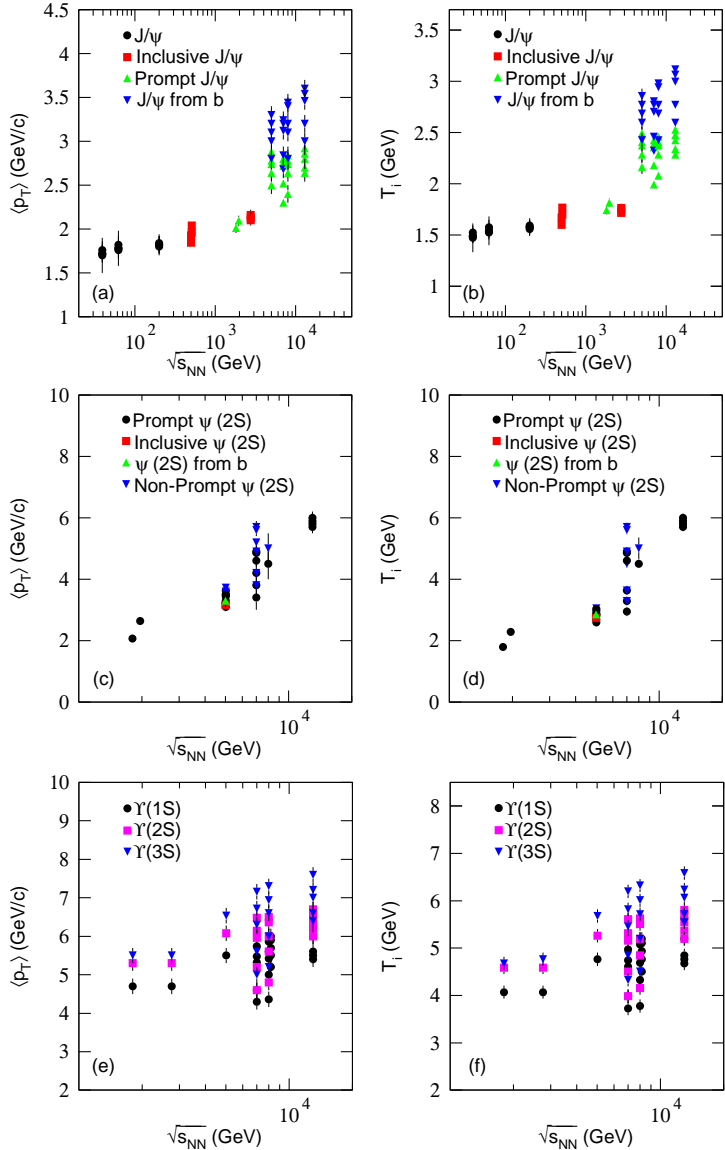


Fig. 7. Dependences of (a)(c)(e) $\langle p_T \rangle$ and (b)(d)(f) T_i on $\sqrt{s_{NN}}$ (or \sqrt{s}) for (a)(b) J/ψ , (c)(d) $\psi(2S)$, and (e)(f) $\Upsilon(nS, n = 1, 2, 3)$. The different symbols represent the parameter values derived from Figs. 1–6 and listed in Tables A1 and A2 where only the (two-component) Erlang distribution in the p_T region of data available is used as an example. By using the mentioned three functions which fit the data good enough in the p_T region of data available, one can obtain similar $\langle p_T \rangle$ (or T_i) within a systematic uncertainty of 8%.

particles. This means that we may use the concept of temperature. Even if the collision system is not enough large, we may use the temperature parameter to characterize the average kinetic energy of given particles over many events.

Figure 7 shows the dependences of (a)(c)(e) $\langle p_T \rangle$ and (b)(d)(f) T_i on $\sqrt{s_{NN}}$ (or \sqrt{s}) for (a)(b) J/ψ , (c)(d) $\psi(2S)$, and (e)(f) $\Upsilon(nS, n = 1, 2, 3)$. The different symbols represent the parameter values derived from free-parameters extracted from Figs. 1–6 and listed in Ta-

bles A1 and A2, where only the (two-component) Erlang distribution in the p_T region of data available is used as an example. It is expected that the results corresponding to the Hagedorn and Tsallis-Levy functions are very close to the plot, because the two functions also describe approximately the data. As what we discussed in subsection 2.5, no matter what functions are used to fit the experimental data, one should obtain similar $\langle p_T \rangle$ (or T_i), if different functions fit the data good enough in the p_T region of data available. By using the men-

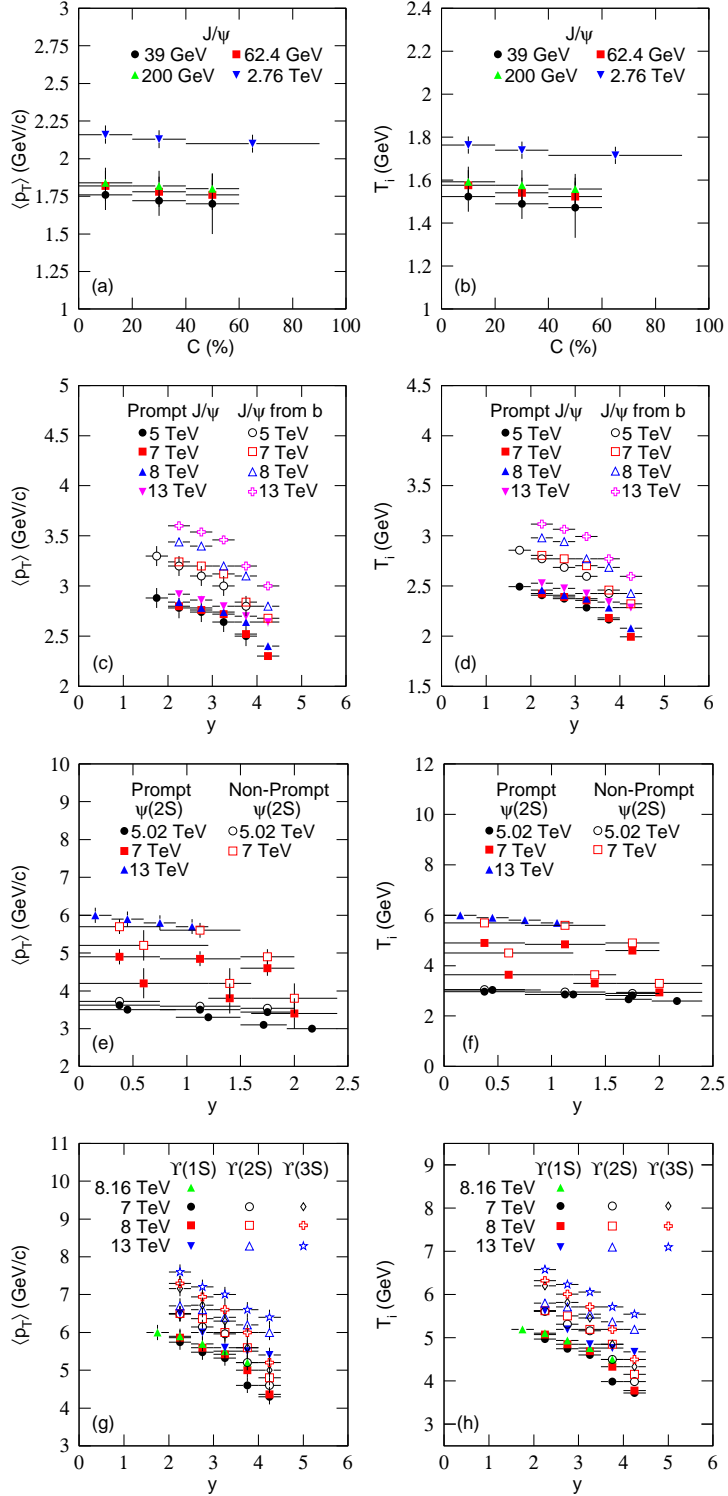


Fig. 8. Same as Fig. 7, but showing the dependences of (a)(c)(e)(g) $\langle p_T \rangle$ and (b)(d)(f)(h) T_i on (a)(b) C and (c)–(h) y for (a)–(d) J/ψ , (e)(f) $\psi(2S)$, and (g)(h) $\Upsilon(nS, n = 1, 2, 3)$.

tioned three functions which fit the data good enough, one can obtain $\langle p_T \rangle$ (or T_i) within a systematic uncertainty of 8%. One can see from Figure 7 that $\langle p_T \rangle$ and

T_i increases significantly with the increase of collision energy. Meanwhile, $\langle p_T \rangle$ and T_i increases with the increase of particle mass.

Figure 8 is the same as Fig. 7, but showing the dependences of (a)(c)(e)(g) $\langle p_T \rangle$ and (b)(d)(f)(h) T_i on (a)(b) centrality C and (c)–(h) rapidity y for (a)–(d) J/ψ , (e)(f) $\psi(2S)$, and (g)(h) $\Upsilon(nS, n = 1, 2, 3)$. The different symbols represent the parameter values derived from free parameters extracted from Figs. 1–6 and listed in Tables A1 and A2, where only the (two-component) Erlang distribution is used as an example. One can see that $\langle p_T \rangle$ and T_i increases slightly with the increase of event centrality from peripheral to central collisions, and decreases with the increase of rapidity from mid-rapidity to forward rapidity. Meanwhile, $\langle p_T \rangle$ and T_i increases with the increases of collision energy and particle mass.

The above parameter tendencies show that the temperature is mass dependent. This is also a reflection of the formation time dependence. According to the hydrodynamic behavior, “massive particles coming out of the system earlier in time with smaller radial flow velocities” [59]. This means that with the increase of mass, the formation time decreases, the temperature increases, and the flow velocity decreases. It should be noted that the fact that the massive particles coming out the system earlier is not caused by the high excitation of the system, but the leaver over due to the inertia of massive particles, in the hydrodynamic evolution.

We may explain the tendency of derived $\langle p_T \rangle$ and T_i which have similar tendency with p_T . With the increase of collision energy, the violent degree of collisions increases significantly due to large energy transfer, which results in the obvious increase of p_T . With the increase of centrality, the degree of multiple-scattering increases due to more participant nucleons and produced particles taking part in the scattering process, which results in slight increase of emission angle and then slight increase of p_T . With the increase of rapidity, the energy transfer decreases due to larger penetrability between participant nucleons. Meanwhile, the degree of multiple-scattering also decreases due to less produced particles taking part in the scattering process. These two factors result in the decrease of p_T . It is natural that p_T increases with the increase of m_0 .

The free parameters in the Erlang distribution are directly reflected in $\langle p_T \rangle$, which will not be discussed anymore. The free parameters in the Hagedorn and Tsallis-Levy functions will be discussed in the Appendix 2, because no clearly physical conclusion can be drawn from them at present, though the tendencies of them can be seen from this work.

4 Summary and conclusions

In summary, the transverse momentum spectra of J/ψ , $\psi(2S)$, and $\Upsilon(nS, n = 1, 2, 3)$ produced in $p+p$, $p+\bar{p}$, $p+Pb$, $Au+Au$, and $Pb+Pb$ collisions over an energy range from 39 GeV to 13 TeV have been analyzed by the (two-component) Erlang distribution, the Hagedorn function, and the Tsallis-Levy function. The function results are approximately in agreement with the experimental data measured by several international collaborations. The values of related parameters are extracted from the fits and the excitation functions of these parameters are obtained.

The excitation functions of parameters $\langle p_T \rangle$ and T_i increase from 39 GeV to 13 TeV. Meanwhile, $\langle p_T \rangle$ and T_i increase (slightly) with event centrality and particle mass and decrease from mid-rapidity to forward rapidity. These tendencies render that these parameters describe the excitation and expansion degrees of the system. At higher energy, larger energy transfer had happened, which results in higher excitation and expansion degrees of the system. In central collisions and at mid-rapidity, larger energy transfer and further multiple-scattering had happened, which also results in higher excitation and expansion degrees of the system.

The parameters $p_0(T)$ and $n_0(n)$ increase with the collision energy, which reflects the degree of energy deposition and transfer. In given collisions, there is a negative correlation between $p_0(T)$ and $n_0(n)$. At different energies, there is a positive correlation between $p_0(T)$ and $n_0(n)$. Indeed, there are correlations between $p_0(T)$ and $n_0(n)$ when we determine these parameters. The correlation between $p_0(T)$ and $n_0(n)$ is similar to that between kinetic freeze-out temperature and transverse flow velocity. If $p_0(T)$ is similar to kinetic freeze-out temperature, $n_0(n)$ should be similar to transverse flow velocity.

Data Availability

The data used to support the findings of this study are included within the article and are cited at relevant places within the text as references.

Ethical Approval

The authors declare that they are in compliance with ethical standards regarding the content of this paper.

Disclosure

The funding agencies have no role in the design of the study; in the collection, analysis, or interpretation

of the data; in the writing of the manuscript; or in the decision to publish the results.

Conflicts of Interest

The authors declare that there are no conflicts of interest regarding the publication of this paper.

Acknowledgments

This work was supported by the National Natural Science Foundation of China under Grant Nos. 11575103 and 11947418, the Scientific and Technological Innovation Programs of Higher Education Institutions in Shanxi (STIP) under Grant No. 201802017, the Shanxi Provincial Natural Science Foundation under Grant No. 201901D111043, and the Fund for Shanxi “1331 Project” Key Subjects Construction.

References

- [1] J. K. Nayak, J. Alam, S. Sarkar, B. Sinha, “Measuring initial temperature through a photon to dilepton ratio in heavy-ion collisions,” *Journal of Physics G*, vol. 35, article 104161, 2008.
- [2] A. Adare et al. [PHENIX Collaboration], “Enhanced production of direct photons in Au+Au collisions at $\sqrt{s_{NN}} = 200$ GeV and implications for the initial temperature,” *Physical Review Letters*, vol. 104, article 132301, 2010.
- [3] M. Csanad and I. Majer, “Initial temperature and EoS of quark matter via direct photons,” *Physics of Particles and Nuclei Letters*, vol 8, pp. 1013–1015, 2011.
- [4] M. Csanad and I. Majer, “Equation of state and initial temperature of quark gluon plasma at RHIC,” *Central European Journal of Physics*, vol. 10, pp. 850–857, 2012.
- [5] R. A. Soltz, I. Garishvili, M. Cheng, B. Abelev, A. Glenn, J. Newby, L. A. L. Levy, and S. Pratt, “Constraining the initial temperature and shear viscosity in a hybrid hydrodynamic model of $\sqrt{s_{NN}} = 200$ GeV Au+Au collisions using pion spectra, elliptic flow, and femtoscopic radii,” *Physical Review C*, vol. 87, article 044901, 2013.
- [6] F.-H. Liu and J.-S. Li, “Isotopic production cross section of fragments in $^{56}\text{Fe}+\text{p}$ and $^{136}\text{Xe}(^{124}\text{Xe})+\text{Pb}$ reactions over an energy range from $300A$ to $1500A$ MeV,” *Physical Review C*, vol. 78, article 044602, 2008.
- [7] F.-H. Liu, “Unified description of multiplicity distributions of final-state particles produced in collisions at high energies,” *Nuclear Physics A*, vol. 810, pp. 159–172, 2008.
- [8] F.-H. Liu, Y.-Q. Gao, T. Tian, B.-C. Li, “Unified description of transverse momentum spectrums contributed by soft and hard processes in high-energy nu-
- clear collisions,” *The European Physical Journal A*, vol. 50, article 94, 2014.
- [9] R. Hagedorn, “Multiplicities, p_T distributions and the expected hadron → quark-gluon phase transition,” *La Rivista del Nuovo Cimento*, vol. 6, no. 10, pp. 1–50 (1983).
- [10] B. Abelev et al. [ALICE Collaboration], “Production of $\Sigma(1385)^{\pm}$ and $\Sigma(1530)^0$ in proton-proton collisions at $\sqrt{s} = 7$ TeV,” *The European Physical Journal C*, vol. 75, article 1, 2015.
- [11] C. Tsallis, “Possible generalization of Boltzmann-Gibbs statistics,” *Journal of Statistical Physics*, vol. 52, pp. 479–487, 1988.
- [12] B. I. Abelev et al. [STAR Collaboration], “Strange particle production in $\text{p}+\text{p}$ collisions at $\sqrt{s} = 200$ GeV,” *Physical Review C*, vol. 75, article 064901, 2007.
- [13] L. Adamczyk et al. [STAR Collaboration], “Energy dependence of J/ψ production in $\text{Au}+\text{Au}$ collisions at $\sqrt{s_{NN}} = 39, 62.4$ and 200 GeV,” *Physics Letters B*, vol. 711, pp. 13–20, 2017.
- [14] J. Adam et al. [STAR Collaboration], “Measurements of the transverse-momentum-dependent cross sections of J/ψ production at mid-rapidity in proton+proton collisions at $\sqrt{s} = 510$ and 500 GeV with the STAR detector,” *Physical Review D*, vol. 100, article 052009, 2019.
- [15] F. Abe et al. [CDF Collaboration], “ J/ψ and $\psi(2S)$ production in $p\bar{p}$ collisions at $\sqrt{s} = 1.8$ TeV,” *Physical Review Letters*, vol. 79, pp. 572–577, 1997.
- [16] D. Acosta et al. [CDF Collaboration], “Measurement of the J/ψ and b -hadron production cross sections in $p\bar{p}$ collisions at $\sqrt{s} = 1960$ GeV,” *Physical Review D*, vol. 71, article 032001, 2005.
- [17] D. Acosta et al. [CDF Collaboration], “ Υ production and polarization in $p\bar{p}$ collisions at $\sqrt{s} = 1.8$ TeV,” *Physical Review Letters*, vol. 88, article 161802, 2002.
- [18] J. Adam et al. [ALICE Collaboration], “Differential studies of inclusive J/ψ and $\psi(2S)$ production at forward rapidity in Pb-Pb collisions at $\sqrt{s_{NN}} = 2.76$ TeV,” *Journal of High Energy Physics*, vol. 16, no. 05, article 179, 2016.
- [19] R. Aaij et al. [LHCb Collaboration], “Study of J/ψ production and cold nuclear matter effects in pPb collisions at $\sqrt{s_{NN}} = 5$ TeV,” *Journal of High Energy Physics*, vol. 14, no. 02, article 072, 2014.
- [20] R. Aaij et al. [LHCb Collaboration], “Measurement of J/ψ production in pp collisions at $\sqrt{s} = 7$ TeV,” *The European Physical Journal C*, vol. 71, article 1645, 2011.
- [21] R. Aaij et al. [LHCb Collaboration], “Production of J/ψ and Υ mesons in pp collisions at $\sqrt{s} = 8$ TeV,” *Journal of High Energy Physics*, vol. 13, no. 06, article 064, 2013.
- [22] R. Aaij et al. [LHCb Collaboration], “Measurement of forward J/ψ production cross-sections in pp collisions at $\sqrt{s} = 13$ TeV,” *Journal of High Energy Physics*, vol. 11, no. 05, article 172, 2015.

- [23] R. Aaij et al. [LHCb Collaboration], “Study of $\psi(2S)$ production and cold nuclear matter effects in $p\text{Pb}$ collisions at $\sqrt{s_{NN}} = 5$ TeV,” *Journal of High Energy Physics*, vol. 16, no. 03, article 133, 2016.
- [24] R. Aaij et al. [LHCb Collaboration], “Measurement of Υ production in pp collisions at $\sqrt{s} = 2.76$ TeV,” *The European Physical Journal C*, vol. 74, article 2835, 2014.
- [25] R. Aaij et al. [LHCb Collaboration], “Forward production of Υ mesons in pp collisions at $\sqrt{s} = 7$ and 8 TeV,” *Journal of High Energy Physics*, vol. 15, no. 11, article 103, 2015.
- [26] R. Aaij et al. [LHCb Collaboration], “Study of Υ production in $p\text{Pb}$ collisions at $\sqrt{s_{NN}} = 8.16$ TeV,” *Journal of High Energy Physics*, vol. 18, no. 11, article 194, 2018.
- [27] R. Aaij et al. [LHCb Collaboration], “Measurement of Υ production in pp collisions at $\sqrt{s} = 13$ TeV,” *Journal of High Energy Physics*, vol. 18, no. 07, article 134, 2018.
- [28] M. Aaboud et al. [ATLAS Collaboration], “Measurement of quarkonium production in proton-lead and proton-proton collisions at 5.02 TeV with the ATLAS detector,” *The European Physical Journal C*, vol. 78, article 171, 2018.
- [29] G. Aad et al. [ATLAS Collaboration], “Measurement of the production cross-section of $\psi(2S) \rightarrow J/\psi(\rightarrow \mu^+ \mu^-) \pi^+ \pi^-$ in pp collisions at $\sqrt{s} = 7$ TeV at ATLAS,” *Journal of High Energy Physics*, vol. 14, no. 09, article 079, 2014.
- [30] M. Aaboud et al. [ATLAS Collaboration], “Measurement of $\psi(2S)$ and $X(3872) \rightarrow J/\psi \pi^+ \pi^-$ production in pp collisions at $\sqrt{s} = 8$ TeV with the ATLAS detector,” *Journal of High Energy Physics*, vol. 17, no. 01, article 117, 2017.
- [31] A. M. Sirunyan et al. [CMS Collaboration], “Measurement of prompt $\psi(2S)$ production cross sections in proton-lead and proton-proton collisions at $\sqrt{s_{NN}} = 5.02$ TeV,” *Physics Letters B*, vol. 790, pp. 509–532, 2019.
- [32] S. Chatrchyan et al. [CMS collaboration], “ J/ψ and $\psi(2S)$ production in pp collisions at $\sqrt{s_{NN}} = 7$ TeV,” *Journal of High Energy Physics*, vol. 12, no. 02, article 011, 2012.
- [33] A. M. Sirunyan et al. [CMS Collaboration], “Measurement of quarkonium production cross sections in pp collisions at $\sqrt{s} = 13$ TeV,” *Physics Letters B*, vol. 780, pp. 251–272, 2018.
- [34] A. M. Sirunyan et al. [CMS Collaboration], “Measurement of nuclear modification factors of $\Upsilon(1S)$, $\Upsilon(2S)$, and $\Upsilon(3S)$ mesons in PbPb collisions at $\sqrt{s_{NN}} = 5.02$ TeV,” *Physics Letters B*, vol. 790, pp. 270–293, 2019.
- [35] E. K. G. Sarkisyan and A. S. Sakharov, “On similarities of bulk observables in nuclear and particle collisions,” CERN-PH-TH-2004-213, arXiv:hep-ph/0410324, 2004.
- [36] E. K. G. Sarkisyan and A. S. Sakharov, “Multihadron production features in different reactions,” *AIP Conference Proceedings*, vol. 828, pp. 35–41, 2006.
- [37] E. K. G. Sarkisyan and A. S. Sakharov, “Relating multihadron production in hadronic and nuclear collisions,” *The European Physical Journal C*, vol. 70, pp. 533–541, 2010.
- [38] E. K. G. Sarkisyan, A. N. Mishra, R. Sahoo, and A. S. Sakharov, “Multihadron production dynamics exploring the energy balance in hadronic and nuclear collisions,” *Physical Review D*, vol. 93, article 054046, 2016.
- [39] E. K. G. Sarkisyan, A. N. Mishra, R. Sahoo, and A. S. Sakharov, “Centrality dependence of midrapidity density from GeV to TeV heavy-ion collisions in the effective-energy universality picture of hadroproduction,” *Physical Review D*, vol. 94, article 011501(R), 2016.
- [40] W. Kittel and E. A. De Wolf, *Soft Multihadron Dynamics*, p. 652. World Scientific, Singapore, 2005.
- [41] R. Nouicer, “Similarity of initial states in $\text{A}+\text{A}$ and $\text{p}+\text{p}$ collisions in constituent quarks framework,” *AIP Conference Proceedings*, vol. 828, pp. 11–16, 2006.
- [42] R. Nouicer for the PHOBOS Collaboration, “Systematic of global observables in $\text{Cu}+\text{Cu}$ and $\text{Au}+\text{Au}$ collisions at RHIC energies,” *AIP Conference Proceedings*, vol. 842, pp. 86–88, 2006.
- [43] R. Nouicer, “Charged particles multiplicities in $\text{A}+\text{A}$ and $\text{p}+\text{p}$ collisions in the constituent quarks framework,” *The European Physical Journal C*, vol. 49, pp. 281–286, 2007.
- [44] J. F. Grosse-Oetringhaus and K. Reygers, “Charged particle multiplicity in proton-proton collisions,” *Journal of Physics G*, vol. 37, article 083001, 2020.
- [45] A. N. Mishra, A. Ortiz, and G. Paić, “Intriguing similarities of high- p_T particle production between pp and AA Collisions,” *Physical Review C*, vol. 99, article 034911, 2019.
- [46] K. Aamodt et al. [ALICE Collaboration], “Transverse momentum spectra of charged particles in proton-proton collisions at $\sqrt{s} = 900$ GeV with ALICE at the LHC,” *Physics Letters B*, vol. 693, pp. 53–68, 2020.
- [47] A. De Falco for the ALICE Collaboration, “Vector meson production in pp collisions at $\sqrt{s} = 7$ TeV, measured with the ALICE detector,” *Journal of Physics G*, vol. 38, article 124083, 2011.
- [48] A. Adare et al. [PHENIX Collaboration], “Nuclear modification factors of ϕ mesons in $\text{d}+\text{Au}$, $\text{Cu}+\text{Cu}$, and $\text{Au}+\text{Au}$ collisions at $\sqrt{s_{NN}} = 200$ GeV,” *Physical Review C*, vol. 83, article 024909, 2011.
- [49] B. Abelev et al. [ALICE Collaboration], “Light vector meson production in pp collisions at $\sqrt{s} = 7$ TeV,” *Physics Letters B*, vol. 710, pp. 557–568, 2012.
- [50] B. Abelev et al. [ALICE Collaboration], “Inclusive J/ψ production in pp collisions at $\sqrt{s} = 2.76$ TeV,” *Physics Letters B*, vol. 718, pp. 295–306, 2012.

- [51] B. Abelev et al. [ALICE Collaboration], “Heavy flavour decay muon production at forward rapidity in proton-proton collisions at $\sqrt{s} = 7$ TeV,” *Physics Letters B*, vol. 708, pp. 265–275, 2012.
- [52] I. Lakomov for the ALICE collaboration, “Event activity dependence of inclusive J/ψ production in p-Pb collisions at $\sqrt{s_{NN}} = 5.02$ TeV with ALICE at the LHC,” *Nuclear Physics A*, vol. 931, pp. 1179–1183, 2014.
- [53] L. G. Gutay, A. S. Hirsch, C. Pajares, R. P. Scharenberg, and B. K. Srivastava, “De-confinement in small systems: Clustering of color sources in high multiplicity $\bar{p}p$ collisions at $\sqrt{s_{NN}} = 1.8$ TeV,” *International Journal of Modern Physics E*, vol. 24, article 1550101, 2015.
- [54] A. S. Hirsch, C. Pajares, R. P. Scharenberg, and B. K. Srivastava, “De-confinement in high multiplicity proton-proton collisions at LHC energies,” *Physical Review D*, vol. 100, article 114040, 2019.
- [55] P. Sahoo, S. De, S. K. Tiwari, and R. Sahoo, “Energy and centrality dependent study of deconfinement phase transition in a color string percolation approach at RHIC energies,” *The European Physical Journal A*, vol. 54, article 136, 2018.
- [56] N. Sarkar, P. Deb, and P. Ghosh, “Finite size effect on thermodynamics of hadron gas in high-multiplicity events of proton-proton collisions at the LHC,” arXiv:1905.06532 [hep-ph], 2019.
- [57] K. Shen, G. G. Barnaföldi, and T. S. Biró, Hadron spectra parameters within the non-extensive approach,” *Universe*, vol 5, article 122, 2019.
- [58] R. Rath, A. Khuntia, and R. Sahoo, “System size and multiplicity dependence of chemical freeze-out parameters at the Large Hadron Collider energies,” arXiv:1905.07959 [hep-ph], 2019.
- [59] R. Sahoo, “Possible formation of QGP-droplets in proton-proton collisions at the CERN Large Hadron Collider,” *AAPPS Bulletin*, vol. 29, no. 4, pp. 16–21, 2019.
- [60] M. Waqas and B.-C. Li, “Kinetic freeze-out temperature and transverse flow velocity in Au-Au collisions at RHIC-BES energies,” *Advances in High Energy Physics*, vol. 2020, article 1787183, 2020.
- [61] P.-P. Yang, M.-Y. Duan, F.-H. Liu, and R. Sahoo, “Multiparticle production and initial quasi-temperature from proton induced carbon collisions at $p_{Lab} = 31$ GeV/c,” *Advances in High Energy Physics*, vol. 2020, article 9542196, 2020.
- [62] Q. Wang and F.-H. Liu, “Initial and final state temperatures of antiproton emission sources in high energy collisions,” *International Journal of Theoretical Physics*, vol. 58, pp. 4119–4138, 2019.

Appendix 1: Tables of parameters.

Table A1. Values of $\langle p_t \rangle_1$, $\langle p_t \rangle_2$, N_1 , k_E , $\langle p_T \rangle$, T_i , and χ^2/ndof corresponding to the solid curves in Figs. 1 and 2. In all cases, $N_2 = 2$ which is not listed in the table. In the case of $\text{ndof} \leq 0$, we use “—” to mention.

Figure	Main selection	$\langle p_t \rangle_1$ (GeV/c)	$\langle p_t \rangle_2$ (GeV/c)	N_1	k_E	$\langle p_T \rangle$ (GeV/c)	T_i (GeV)	χ^2/ndof
1(a)	0–20%	0.88 ± 0.05	—	2 ± 0	1	1.760 ± 0.100	1.520 ± 0.070	1.87/—
	20–40%	0.86 ± 0.05	—	2 ± 0	1	1.720 ± 0.100	1.490 ± 0.070	1.67/—
	40–60%	0.85 ± 0.10	—	2 ± 0	1	1.700 ± 0.200	1.472 ± 0.140	0.38/—
	0–60%	0.86 ± 0.05	—	2 ± 0	1	1.720 ± 0.100	1.490 ± 0.070	1.34/—
1(b)	0–20%	0.91 ± 0.05	—	2 ± 0	1	1.820 ± 0.100	1.576 ± 0.070	2.10/—
	20–40%	0.89 ± 0.05	—	2 ± 0	1	1.780 ± 0.100	1.542 ± 0.070	1.05/—
	40–60%	0.88 ± 0.05	—	2 ± 0	1	1.760 ± 0.100	1.524 ± 0.070	2.64/—
	0–60%	0.89 ± 0.01	—	2 ± 0	1	1.780 ± 0.200	1.542 ± 0.140	2.81/—
1(c)	0–20%	0.92 ± 0.05	—	2 ± 0	1	1.840 ± 0.100	1.593 ± 0.070	0.66/2
	20–40%	0.91 ± 0.05	—	2 ± 0	1	1.820 ± 0.100	1.576 ± 0.070	2.47/2
	40–60%	0.90 ± 0.05	—	2 ± 0	1	1.800 ± 0.100	1.559 ± 0.070	2.65/2
	0–60%	0.91 ± 0.05	—	2 ± 0	1	1.820 ± 0.100	1.576 ± 0.070	1.99/2
1(d)	Full cross section	0.91 ± 0.02	2.20 ± 0.05	2 ± 0	0.99 ± 0.01	1.846 ± 0.034	1.663 ± 0.037	13.40/14
	Fiducial cross section	0.95 ± 0.01	2.50 ± 0.05	2 ± 0	0.99 ± 0.01	1.931 ± 0.030	1.709 ± 0.040	54.91/14
1(e)	Full cross section	0.98 ± 0.02	—	2 ± 0	1	1.960 ± 0.040	1.697 ± 0.030	5.50/2
	Fiducial cross section	1.02 ± 0.02	—	2 ± 0	1	2.040 ± 0.040	1.767 ± 0.030	14.50/2
1(f)	1.8 TeV	0.98 ± 0.05	2.30 ± 0.10	2 ± 0	0.98 ± 0.01	2.013 ± 0.056	1.743 ± 0.040	6.54/6
	1.96 TeV	1.02 ± 0.05	2.41 ± 0.10	2 ± 0	0.98 ± 0.01	2.096 ± 0.057	1.815 ± 0.041	17.34/19
1(g)	0–20%	0.72 ± 0.02	—	3 ± 0	1	2.160 ± 0.060	1.764 ± 0.040	25.90/10
	20–40%	0.71 ± 0.02	—	3 ± 0	1	2.130 ± 0.060	1.739 ± 0.040	20.90/10
	40–90%	0.70 ± 0.02	—	3 ± 0	1	2.100 ± 0.060	1.715 ± 0.040	30.75/10
2(a)	1.5 < y < 2.0	1.44 ± 0.05	—	2 ± 0	1	2.880 ± 0.100	2.494 ± 0.035	4.00/5
	2.0 < y < 2.5	1.39 ± 0.05	—	2 ± 0	1	2.780 ± 0.100	2.408 ± 0.035	4.40/5
	2.5 < y < 3.0	1.37 ± 0.05	—	2 ± 0	1	2.740 ± 0.100	2.373 ± 0.035	3.95/5
	3.0 < y < 3.5	1.32 ± 0.05	—	2 ± 0	1	2.640 ± 0.100	2.286 ± 0.035	3.96/5
	3.5 < y < 4.0	1.25 ± 0.05	—	2 ± 0	1	2.500 ± 0.100	2.165 ± 0.035	4.84/5
2(b)	1.5 < y < 2.0	1.65 ± 0.05	—	2 ± 0	1	3.300 ± 0.100	2.858 ± 0.035	3.01/5
	2.0 < y < 2.5	1.60 ± 0.05	—	2 ± 0	1	3.200 ± 0.100	2.771 ± 0.035	5.99/5
	2.5 < y < 3.0	1.55 ± 0.05	—	2 ± 0	1	3.100 ± 0.100	2.685 ± 0.035	8.89/5
	3.0 < y < 3.5	1.50 ± 0.05	—	2 ± 0	1	3.000 ± 0.100	2.598 ± 0.035	11.77/5
	3.5 < y < 4.0	1.40 ± 0.05	—	2 ± 0	1	2.800 ± 0.100	2.425 ± 0.035	13.44/5
2(c)	2.0 < y < 2.5	1.40 ± 0.02	—	2 ± 0	1	2.800 ± 0.040	2.425 ± 0.014	10.37/11
	2.5 < y < 3.0	1.38 ± 0.02	—	2 ± 0	1	2.760 ± 0.040	2.390 ± 0.014	10.43/11
	3.0 < y < 3.5	1.36 ± 0.02	—	2 ± 0	1	2.720 ± 0.040	2.356 ± 0.014	10.12/11
	3.5 < y < 4.0	1.26 ± 0.02	—	2 ± 0	1	2.520 ± 0.040	2.182 ± 0.014	7.96/10
2(d)	4.0 < y < 4.5	1.15 ± 0.02	—	2 ± 0	1	2.300 ± 0.040	1.992 ± 0.014	5.97/8
	2.0 < y < 2.5	1.62 ± 0.02	—	2 ± 0	1	3.240 ± 0.040	2.806 ± 0.014	7.49/11
	2.5 < y < 3.0	1.60 ± 0.02	—	2 ± 0	1	3.200 ± 0.040	2.771 ± 0.014	7.18/11
	3.0 < y < 3.5	1.56 ± 0.02	—	2 ± 0	1	3.120 ± 0.040	2.702 ± 0.014	8.82/11
2(e)	3.5 < y < 4.0	1.42 ± 0.02	—	2 ± 0	1	2.840 ± 0.040	2.460 ± 0.014	5.13/10
	4.0 < y < 4.5	1.34 ± 0.02	—	2 ± 0	1	2.680 ± 0.040	2.321 ± 0.014	6.36/8
	2.0 < y < 2.5	1.42 ± 0.02	—	2 ± 0	1	2.840 ± 0.040	2.460 ± 0.014	9.57/11
	2.5 < y < 3.0	1.39 ± 0.02	—	2 ± 0	1	2.780 ± 0.040	2.408 ± 0.014	7.10/11
2(f)	3.0 < y < 3.5	1.37 ± 0.02	—	2 ± 0	1	2.740 ± 0.040	2.373 ± 0.014	9.77/11
	3.5 < y < 4.0	1.32 ± 0.02	—	2 ± 0	1	2.640 ± 0.040	2.286 ± 0.014	9.62/11
	4.0 < y < 4.5	1.20 ± 0.02	—	2 ± 0	1	2.400 ± 0.040	2.078 ± 0.014	7.60/11
	2.0 < y < 2.5	1.72 ± 0.02	—	2 ± 0	1	3.440 ± 0.040	2.979 ± 0.014	8.11/11
2(g)	2.5 < y < 3.0	1.70 ± 0.02	—	2 ± 0	1	3.400 ± 0.040	2.944 ± 0.014	8.99/11
	3.0 < y < 3.5	1.60 ± 0.02	—	2 ± 0	1	3.200 ± 0.040	2.771 ± 0.014	9.57/11
	3.5 < y < 4.0	1.55 ± 0.02	—	2 ± 0	1	3.100 ± 0.040	2.685 ± 0.014	9.89/11
	4.0 < y < 4.5	1.40 ± 0.02	—	2 ± 0	1	2.800 ± 0.040	2.425 ± 0.014	7.99/11
2(h)	2.0 < y < 2.5	1.80 ± 0.02	—	2 ± 0	1	3.600 ± 0.040	3.118 ± 0.014	10.58/11
	2.5 < y < 3.0	1.77 ± 0.02	—	2 ± 0	1	3.540 ± 0.040	3.066 ± 0.014	9.08/11
	3.0 < y < 3.5	1.73 ± 0.02	—	2 ± 0	1	3.460 ± 0.040	2.996 ± 0.014	9.17/11
	3.5 < y < 4.0	1.60 ± 0.02	—	2 ± 0	1	3.200 ± 0.040	2.771 ± 0.014	9.47/11
	4.0 < y < 4.5	1.50 ± 0.02	—	2 ± 0	1	3.000 ± 0.040	2.598 ± 0.014	12.09/11

Table A1. Continued. Values of $\langle p_t \rangle_1$, $\langle p_t \rangle_2$, N_1 , k_E , $\langle p_T \rangle$, T_i , and χ^2/ndof corresponding to the solid curves in Figs. 3 and 4. In all cases, $N_2 = 2$ which is not listed in the table. In the case of $\text{ndof} \leq 0$, we use “–” to mention.

Figure	Main selection	$\langle p_t \rangle_1$ (GeV/c)	$\langle p_t \rangle_2$ (GeV/c)	N_1	k_E	$\langle p_T \rangle$ (GeV/c)	T_i (GeV)	χ^2/ndof
3(a)	1.8 TeV	1.00 ± 0.05	2.70 ± 0.20	2 ± 0	0.98 ± 0.01	2.068 ± 0.060	1.791 ± 0.045	$3.80/-$
	1.96 TeV	1.30 ± 0.05	3.30 ± 0.10	2 ± 0	0.99 ± 0.01	2.640 ± 0.064	2.286 ± 0.055	$11.16/20$
3(b)	Inclusive $\psi(2S)$	1.58 ± 0.10	–	2 ± 0	1	3.160 ± 0.200	2.737 ± 0.071	$13.01/2$
	Prompt $\psi(2S)$	1.61 ± 0.05	–	2 ± 0	1	3.220 ± 0.100	2.789 ± 0.035	$5.49/2$
	$\psi(2S)$ from b	1.65 ± 0.10	–	2 ± 0	1	3.300 ± 0.200	2.858 ± 0.071	$8.51/2$
3(c)	$0.00 < y < 0.75$	1.18 ± 0.03	3.75 ± 0.20	3 ± 0	0.98 ± 0.01	3.619 ± 0.069	2.962 ± 0.074	$2.39/-$
	$0.75 < y < 1.50$	1.14 ± 0.02	3.65 ± 0.05	3 ± 0	0.98 ± 0.01	3.498 ± 0.056	2.863 ± 0.070	$3.50/-$
	$1.50 < y < 2.00$	1.12 ± 0.01	3.60 ± 0.05	3 ± 0	0.98 ± 0.01	3.437 ± 0.046	2.813 ± 0.069	$4.25/-$
3(d)	$0.00 < y < 0.75$	1.20 ± 0.03	3.80 ± 0.10	3 ± 0	0.97 ± 0.01	3.720 ± 0.068	3.049 ± 0.074	$3.23/-$
	$0.75 < y < 1.50$	1.16 ± 0.03	3.70 ± 0.10	3 ± 0	0.97 ± 0.01	3.598 ± 0.067	2.948 ± 0.072	$7.64/-$
	$1.50 < y < 2.00$	1.14 ± 0.03	3.65 ± 0.10	3 ± 0	0.97 ± 0.01	3.536 ± 0.049	2.898 ± 0.071	$2.33/-$
3(e)	$0 < y < 0.9$	3.50 ± 0.10	–	1 ± 0	1	3.500 ± 0.100	3.031 ± 0.035	$1.45/-$
	$0.9 < y < 1.5$	3.30 ± 0.10	–	1 ± 0	1	3.300 ± 0.100	2.858 ± 0.035	$1.81/-$
	$1.5 < y < 1.93$	3.10 ± 0.10	–	1 ± 0	1	3.100 ± 0.100	2.685 ± 0.035	$2.75/-$
3(f)	$ y < 1.2$	2.10 ± 0.20	–	2 ± 0	1	4.200 ± 0.040	3.637 ± 0.141	$4.51/6$
	$1.2 < y < 1.6$	1.90 ± 0.20	–	2 ± 0	1	3.800 ± 0.040	3.291 ± 0.141	$6.30/4$
	$1.6 < y < 2.4$	1.70 ± 0.20	–	2 ± 0	1	3.400 ± 0.040	2.944 ± 0.141	$5.71/4$
3(g)	$ y < 1.2$	2.60 ± 0.20	–	2 ± 0	1	5.200 ± 0.040	4.503 ± 0.141	$4.19/6$
	$1.2 < y < 1.6$	2.10 ± 0.20	–	2 ± 0	1	4.200 ± 0.040	3.637 ± 0.141	$6.61/4$
	$1.6 < y < 2.4$	1.90 ± 0.20	–	2 ± 0	1	3.800 ± 0.040	3.291 ± 0.141	$5.58/4$
4(a)	$ y < 0.75$	4.90 ± 0.20	–	1 ± 0	1	4.900 ± 0.200	4.900 ± 0.141	$16.68/7$
	$0.75 < y < 1.5$	4.85 ± 0.20	–	1 ± 0	1	4.850 ± 0.200	4.850 ± 0.141	$12.64/7$
	$1.5 < y < 2.0$	4.60 ± 0.20	–	1 ± 0	1	4.600 ± 0.200	4.600 ± 0.141	$14.92/7$
4(b)	$ y < 0.75$	5.70 ± 0.20	–	1 ± 0	1	5.700 ± 0.200	5.700 ± 0.141	$9.50/7$
	$0.75 < y < 1.5$	5.60 ± 0.20	–	1 ± 0	1	5.600 ± 0.200	5.600 ± 0.141	$12.60/7$
	$1.5 < y < 2.0$	4.90 ± 0.20	–	1 ± 0	1	4.900 ± 0.200	4.900 ± 0.141	$23.39/7$
4(c)	Prompt $\psi(2S)$	4.50 ± 0.50	–	1 ± 0	1	4.500 ± 0.500	4.500 ± 0.354	$31.00/2$
	Non-prompt $\psi(2S)$	5.00 ± 0.50	–	1 ± 0	1	5.000 ± 0.500	5.000 ± 0.354	$24.00/2$
4(d)	$0.0 < y < 0.3$	6.00 ± 0.20	–	1 ± 0	1	6.000 ± 0.200	6.000 ± 0.141	$78.14/6$
	$0.3 < y < 0.6$	5.90 ± 0.20	–	1 ± 0	1	5.900 ± 0.200	5.900 ± 0.141	$149.64/6$
	$0.6 < y < 0.9$	5.80 ± 0.20	–	1 ± 0	1	5.800 ± 0.200	5.800 ± 0.141	$191.75/6$
4(d)	$0.9 < y < 1.2$	5.70 ± 0.20	–	1 ± 0	1	5.700 ± 0.200	5.700 ± 0.141	$444.14/6$

Table A1. Continued. Values of $\langle p_t \rangle_1$, $\langle p_t \rangle_2$, N_1 , k_E , $\langle p_T \rangle$, T_i , and χ^2/ndof corresponding to the solid curves in Figs. 5 and 6. In all cases, $N_2 = 2$ which is not listed in the table. In the case of $\text{ndof} \leq 0$, we use “–” to mention.

Figure	Main selection	$\langle p_t \rangle_1$ (GeV/c)	$\langle p_t \rangle_2$ (GeV/c)	N_1	k_E	$\langle p_T \rangle$ (GeV/c)	T_i (GeV)	χ^2/ndof
5(a)	$\Upsilon(1S)$	2.35 ± 0.10	–	2 ± 0	1	4.700 ± 0.200	4.070 ± 0.071	14.28/11
	$\Upsilon(2S)$	2.65 ± 0.10	–	2 ± 0	1	5.300 ± 0.200	4.590 ± 0.071	11.50/6
	$\Upsilon(3S)$	2.70 ± 0.10	–	2 ± 0	1	5.400 ± 0.200	4.677 ± 0.071	7.99/6
5(b)	$\Upsilon(1S)$	2.35 ± 0.10	–	2 ± 0	1	4.700 ± 0.200	4.070 ± 0.071	7.79/3
	$\Upsilon(2S)$	2.65 ± 0.10	–	2 ± 0	1	5.300 ± 0.200	4.590 ± 0.071	4.25/3
	$\Upsilon(3S)$	2.75 ± 0.10	–	2 ± 0	1	5.500 ± 0.200	4.763 ± 0.071	2.36/3
5(c)	$\Upsilon(1S)$	2.75 ± 0.10	–	2 ± 0	1	5.500 ± 0.200	4.763 ± 0.071	13.89/3
	$\Upsilon(2S)$	3.04 ± 0.10	–	2 ± 0	1	6.080 ± 0.200	5.265 ± 0.071	11.00/–
	$\Upsilon(3S)$	3.28 ± 0.10	–	2 ± 0	1	6.540 ± 0.200	5.681 ± 0.071	12.00/–
5(d)	$2.0 < y < 2.5$	2.87 ± 0.10	–	2 ± 0	1	5.740 ± 0.200	4.971 ± 0.071	10.30/21
	$2.5 < y < 3.0$	2.74 ± 0.10	–	2 ± 0	1	5.480 ± 0.200	4.746 ± 0.071	12.57/21
	$3.0 < y < 3.5$	2.66 ± 0.10	–	2 ± 0	1	5.320 ± 0.200	4.607 ± 0.071	13.98/21
	$3.5 < y < 4.0$	2.30 ± 0.10	–	2 ± 0	1	4.600 ± 0.200	3.984 ± 0.071	11.90/18
	$4.0 < y < 4.5$	2.15 ± 0.10	–	2 ± 0	1	4.300 ± 0.200	3.724 ± 0.071	8.28/12
	$2.0 < y < 2.5$	3.24 ± 0.10	–	2 ± 0	1	6.480 ± 0.200	5.612 ± 0.071	14.04/21
5(e)	$2.5 < y < 3.0$	3.07 ± 0.10	–	2 ± 0	1	6.140 ± 0.200	5.317 ± 0.071	11.76/21
	$3.0 < y < 3.5$	2.98 ± 0.10	–	2 ± 0	1	5.960 ± 0.200	5.162 ± 0.071	10.98/21
	$3.5 < y < 4.0$	2.60 ± 0.10	–	2 ± 0	1	5.200 ± 0.200	4.503 ± 0.071	9.67/18
	$4.0 < y < 4.5$	2.30 ± 0.10	–	2 ± 0	1	4.600 ± 0.200	3.984 ± 0.071	9.78/12
	$2.0 < y < 2.5$	3.58 ± 0.10	–	2 ± 0	1	7.160 ± 0.200	6.201 ± 0.071	10.56/21
	$2.5 < y < 3.0$	3.36 ± 0.10	–	2 ± 0	1	6.720 ± 0.200	5.820 ± 0.071	8.31/21
5(f)	$3.0 < y < 3.5$	3.15 ± 0.10	–	2 ± 0	1	6.300 ± 0.200	5.456 ± 0.071	10.95/21
	$3.5 < y < 4.0$	2.80 ± 0.10	–	2 ± 0	1	5.600 ± 0.200	4.850 ± 0.071	10.59/18
	$4.0 < y < 4.5$	2.50 ± 0.10	–	2 ± 0	1	5.000 ± 0.200	4.330 ± 0.071	9.28/12
	$2.0 < y < 2.5$	2.93 ± 0.10	–	2 ± 0	1	5.860 ± 0.200	5.075 ± 0.071	13.98/21
	$2.5 < y < 3.0$	2.80 ± 0.10	–	2 ± 0	1	5.600 ± 0.200	4.850 ± 0.071	17.21/21
	$3.0 < y < 3.5$	2.71 ± 0.10	–	2 ± 0	1	5.420 ± 0.200	4.694 ± 0.071	15.08/21
6(b)	$3.5 < y < 4.0$	2.50 ± 0.10	–	2 ± 0	1	5.000 ± 0.200	4.330 ± 0.071	7.56/18
	$4.0 < y < 4.5$	2.18 ± 0.10	–	2 ± 0	1	4.360 ± 0.200	3.776 ± 0.071	8.70/12
	$2.0 < y < 2.5$	3.25 ± 0.10	–	2 ± 0	1	6.500 ± 0.200	5.629 ± 0.071	13.31/21
	$2.5 < y < 3.0$	3.18 ± 0.10	–	2 ± 0	1	6.360 ± 0.200	5.508 ± 0.071	15.28/21
	$3.0 < y < 3.5$	3.00 ± 0.10	–	2 ± 0	1	6.000 ± 0.200	5.196 ± 0.071	12.05/21
	$3.5 < y < 4.0$	2.80 ± 0.10	–	2 ± 0	1	5.600 ± 0.200	4.850 ± 0.071	10.23/18
6(c)	$4.0 < y < 4.5$	2.40 ± 0.10	–	2 ± 0	1	4.800 ± 0.200	4.157 ± 0.071	9.45/12
	$2.0 < y < 2.5$	3.65 ± 0.10	–	2 ± 0	1	7.300 ± 0.200	6.322 ± 0.071	10.23/21
	$2.5 < y < 3.0$	3.47 ± 0.10	–	2 ± 0	1	6.940 ± 0.200	6.010 ± 0.071	12.87/21
	$3.0 < y < 3.5$	3.30 ± 0.10	–	2 ± 0	1	6.600 ± 0.200	5.716 ± 0.071	9.25/21
	$3.5 < y < 4.0$	3.00 ± 0.10	–	2 ± 0	1	6.000 ± 0.200	5.196 ± 0.071	7.25/18
	$4.0 < y < 4.5$	2.60 ± 0.10	–	2 ± 0	1	5.200 ± 0.200	4.503 ± 0.071	9.06/12
6(d)	$1.5 < y < 2.0$	3.00 ± 0.10	–	2 ± 0	1	6.000 ± 0.200	5.196 ± 0.071	4.47/4
	$2.0 < y < 2.5$	2.95 ± 0.10	–	2 ± 0	1	5.900 ± 0.200	5.110 ± 0.083	2.43/4
	$2.5 < y < 3.0$	2.85 ± 0.10	–	2 ± 0	1	5.700 ± 0.200	4.936 ± 0.082	3.25/4
	$3.0 < y < 3.5$	2.75 ± 0.10	–	2 ± 0	1	5.500 ± 0.200	4.763 ± 0.081	3.64/4
	$3.5 < y < 4.0$	2.60 ± 0.10	–	2 ± 0	1	5.200 ± 0.200	4.503 ± 0.071	4.52/3
	$2.0 < y < 2.5$	3.25 ± 0.10	–	2 ± 0	1	6.500 ± 0.200	5.629 ± 0.071	18.79/21
6(e)	$2.5 < y < 3.0$	3.00 ± 0.10	–	2 ± 0	1	6.000 ± 0.200	5.196 ± 0.071	17.87/22
	$3.0 < y < 3.5$	2.80 ± 0.10	–	2 ± 0	1	5.600 ± 0.200	4.850 ± 0.071	18.85/21
	$3.5 < y < 4.0$	2.75 ± 0.10	–	2 ± 0	1	5.500 ± 0.200	4.763 ± 0.071	16.42/19
	$4.0 < y < 4.5$	2.70 ± 0.10	–	2 ± 0	1	5.400 ± 0.200	4.677 ± 0.071	11.03/13
	$2.0 < y < 2.5$	3.35 ± 0.10	–	2 ± 0	1	6.700 ± 0.200	5.802 ± 0.071	17.71/21
	$2.5 < y < 3.0$	3.30 ± 0.10	–	2 ± 0	1	6.600 ± 0.200	5.716 ± 0.071	23.75/22
6(f)	$3.0 < y < 3.5$	3.20 ± 0.10	–	2 ± 0	1	6.400 ± 0.200	5.543 ± 0.071	16.94/21
	$3.5 < y < 4.0$	3.10 ± 0.10	–	2 ± 0	1	6.200 ± 0.200	5.369 ± 0.071	20.21/19
	$4.0 < y < 4.5$	3.00 ± 0.10	–	2 ± 0	1	6.000 ± 0.200	5.196 ± 0.071	10.58/13
	$2.0 < y < 2.5$	3.80 ± 0.10	–	2 ± 0	1	7.600 ± 0.200	6.582 ± 0.071	13.87/21
	$2.5 < y < 3.0$	3.60 ± 0.10	–	2 ± 0	1	7.200 ± 0.200	6.235 ± 0.071	14.69/22
	$3.0 < y < 3.5$	3.50 ± 0.10	–	2 ± 0	1	7.000 ± 0.200	6.062 ± 0.071	12.10/21
6(g)	$3.5 < y < 4.0$	3.30 ± 0.10	–	2 ± 0	1	6.600 ± 0.200	5.716 ± 0.071	16.61/19
	$4.0 < y < 4.5$	3.20 ± 0.10	–	2 ± 0	1	6.400 ± 0.200	5.543 ± 0.071	11.17/13

Table A2. Values of p_0 , n_0 , and χ^2/ndof corresponding to the dashed curves in Figs. 1 and 2, as well as values of T , n , and χ^2/ndof corresponding to the dotted curves in Figs. 1 and 2.

Figure	Main selection	p_0 (GeV/c)	n_0	χ^2/ndof	T (GeV)	n	χ^2/ndof
1(a)	0–20%	6.20 ± 0.50	7.80 ± 0.50	1.07/–	0.39 ± 0.02	5.70 ± 1.00	0.80/–
	20–40%	6.10 ± 0.50	7.90 ± 0.50	2.11/–	0.37 ± 0.02	6.00 ± 1.00	1.01/–
	40–60%	5.95 ± 0.50	8.05 ± 0.50	0.23/–	0.36 ± 0.02	6.20 ± 1.00	1.11/–
	0–60%	6.00 ± 0.50	8.00 ± 0.50	0.59/–	0.37 ± 0.02	6.00 ± 1.00	0.44/–
1(b)	0–20%	6.60 ± 0.50	8.00 ± 0.50	3.00/–	0.41 ± 0.02	5.90 ± 1.00	1.40/–
	20–40%	6.50 ± 0.50	8.10 ± 0.50	1.73/–	0.39 ± 0.02	6.20 ± 1.00	1.07/–
	40–60%	6.35 ± 0.50	8.25 ± 0.50	2.16/–	0.38 ± 0.02	6.30 ± 1.00	0.78/–
	0–60%	6.40 ± 0.30	8.20 ± 0.30	2.94/–	0.39 ± 0.02	6.20 ± 1.00	1.37/–
1(c)	0–20%	7.00 ± 0.50	9.30 ± 0.50	2.36/2	0.43 ± 0.02	6.10 ± 1.00	0.84/2
	20–40%	6.80 ± 0.20	9.50 ± 0.20	4.43/2	0.40 ± 0.02	6.30 ± 1.00	1.86/2
	40–60%	6.70 ± 0.50	9.60 ± 0.50	3.85/2	0.39 ± 0.02	6.40 ± 1.00	1.46/2
	0–60%	6.80 ± 0.50	9.50 ± 0.50	3.86/2	0.40 ± 0.02	6.30 ± 1.00	0.41/2
1(d)	Full cross section	6.80 ± 0.30	11.50 ± 0.30	35.57/16	0.44 ± 0.02	8.00 ± 0.20	24.30/16
	Fiducial cross section	7.00 ± 0.30	11.00 ± 0.30	70.35/16	0.47 ± 0.01	7.50 ± 0.20	54.75/16
1(e)	Full cross section	7.50 ± 0.50	11.70 ± 1.00	11.89/2	0.45 ± 0.02	8.10 ± 1.00	2.22/2
	Fiducial cross section	8.00 ± 0.30	11.20 ± 0.50	4.31/2	0.50 ± 0.03	7.60 ± 1.00	10.25/2
1(f)	1.8 TeV	8.10 ± 0.30	11.80 ± 0.30	4.87/8	0.55 ± 0.02	8.50 ± 0.20	4.20/8
	1.96 TeV	8.20 ± 0.30	12.00 ± 0.50	26.09/21	0.57 ± 0.03	8.90 ± 0.50	21.40/21
1(g)	0–20%	12.40 ± 0.50	11.50 ± 0.50	217.00/10	0.53 ± 0.05	11.50 ± 2.00	11.31/10
	20–40%	12.20 ± 0.50	11.80 ± 0.50	90.75/10	0.52 ± 0.05	11.60 ± 2.00	10.92/10
	40–90%	12.00 ± 0.50	12.00 ± 0.50	41.80/10	0.52 ± 0.05	11.65 ± 2.00	15.71/10
2(a)	$1.5 < y < 2.0$	13.00 ± 0.50	12.50 ± 0.50	8.97/5	0.85 ± 0.05	10.00 ± 2.00	2.16/5
	$2.0 < y < 2.5$	12.90 ± 0.50	12.60 ± 0.50	8.52/5	0.84 ± 0.05	10.50 ± 2.00	2.66/5
	$2.5 < y < 3.0$	12.60 ± 0.50	12.90 ± 0.50	5.91/5	0.83 ± 0.05	11.00 ± 2.00	2.46/5
	$3.0 < y < 3.5$	12.40 ± 0.50	13.10 ± 0.50	5.91/5	0.82 ± 0.05	11.50 ± 2.00	3.10/5
	$3.5 < y < 4.0$	12.10 ± 0.50	13.50 ± 0.50	5.85/5	0.80 ± 0.05	12.50 ± 2.00	3.61/5
2(b)	$1.5 < y < 2.0$	14.50 ± 0.50	12.00 ± 0.50	3.10/5	1.00 ± 0.10	9.50 ± 2.00	3.65/5
	$2.0 < y < 2.5$	14.40 ± 0.50	12.10 ± 0.50	3.75/5	0.98 ± 0.05	9.70 ± 2.00	3.62/5
	$2.5 < y < 3.0$	14.30 ± 0.50	12.20 ± 0.50	6.39/5	0.95 ± 0.05	10.00 ± 2.00	4.60/5
	$3.0 < y < 3.5$	14.10 ± 0.50	12.40 ± 0.50	6.75/5	0.93 ± 0.05	10.20 ± 2.00	6.60/5
	$3.5 < y < 4.0$	13.50 ± 0.50	13.00 ± 0.50	11.66/5	0.87 ± 0.05	11.00 ± 2.00	5.21/5
2(c)	$2.0 < y < 2.5$	13.50 ± 0.50	14.00 ± 0.50	8.91/11	0.85 ± 0.05	12.50 ± 2.00	7.93/11
	$2.5 < y < 3.0$	13.30 ± 0.50	14.20 ± 0.50	8.66/11	0.84 ± 0.05	13.00 ± 2.00	9.52/11
	$3.0 < y < 3.5$	13.00 ± 0.50	14.40 ± 0.50	8.41/11	0.82 ± 0.05	14.00 ± 2.00	9.55/11
	$3.5 < y < 4.0$	12.60 ± 0.50	14.80 ± 0.50	8.30/10	0.80 ± 0.05	15.00 ± 2.00	8.99/10
	$4.0 < y < 4.5$	12.20 ± 0.50	15.00 ± 0.50	7.80/8	0.74 ± 0.05	16.00 ± 2.00	4.91/8
2(d)	$2.0 < y < 2.5$	15.00 ± 0.50	13.00 ± 0.50	3.19/11	1.02 ± 0.05	11.00 ± 2.00	5.85/11
	$2.5 < y < 3.0$	14.80 ± 0.50	13.20 ± 0.50	4.93/11	1.00 ± 0.05	11.50 ± 2.00	6.44/11
	$3.0 < y < 3.5$	14.30 ± 0.50	13.50 ± 0.50	5.32/11	0.98 ± 0.05	12.00 ± 2.00	5.98/11
	$3.5 < y < 4.0$	14.10 ± 0.50	14.00 ± 0.50	8.86/10	0.93 ± 0.05	13.00 ± 2.00	6.55/10
	$4.0 < y < 4.5$	14.00 ± 0.50	14.20 ± 0.50	9.91/8	0.90 ± 0.05	13.50 ± 2.00	5.26/8
2(e)	$2.0 < y < 2.5$	13.70 ± 0.50	14.20 ± 0.50	10.12/11	0.88 ± 0.05	13.00 ± 2.00	7.17/11
	$2.5 < y < 3.0$	13.50 ± 0.50	14.40 ± 0.50	5.75/11	0.87 ± 0.05	13.50 ± 2.00	8.75/11
	$3.0 < y < 3.5$	13.30 ± 0.50	14.60 ± 0.50	5.78/11	0.86 ± 0.05	14.00 ± 2.00	8.16/11
	$3.5 < y < 4.0$	13.10 ± 0.50	14.80 ± 0.50	8.76/11	0.84 ± 0.05	15.00 ± 2.00	10.56/11
	$4.0 < y < 4.5$	12.50 ± 0.50	15.20 ± 0.50	9.92/11	0.77 ± 0.05	16.50 ± 2.00	7.25/11
2(f)	$2.0 < y < 2.5$	15.60 ± 0.50	13.10 ± 0.50	5.45/11	1.07 ± 0.05	11.50 ± 2.00	5.17/11
	$2.5 < y < 3.0$	15.40 ± 0.50	13.30 ± 0.50	8.64/11	1.05 ± 0.05	12.00 ± 2.00	6.79/11
	$3.0 < y < 3.5$	15.00 ± 0.50	13.70 ± 0.50	5.17/11	1.02 ± 0.05	12.50 ± 2.00	7.16/11
	$3.5 < y < 4.0$	14.70 ± 0.50	14.10 ± 0.50	11.56/11	0.98 ± 0.05	13.50 ± 2.00	7.07/11
	$4.0 < y < 4.5$	14.20 ± 0.50	14.40 ± 0.50	9.57/11	0.93 ± 0.05	14.00 ± 2.00	5.81/11
2(g)	$2.0 < y < 2.5$	15.30 ± 0.50	14.80 ± 0.50	9.38/11	0.93 ± 0.05	14.00 ± 2.00	6.16/11
	$2.5 < y < 3.0$	15.20 ± 0.50	14.90 ± 0.50	8.95/11	0.91 ± 0.05	14.50 ± 2.00	8.12/11
	$3.0 < y < 3.5$	15.00 ± 0.50	15.00 ± 0.50	7.32/11	0.89 ± 0.05	14.80 ± 2.00	9.17/11
	$3.5 < y < 4.0$	14.40 ± 0.50	15.30 ± 0.50	11.22/11	0.86 ± 0.05	15.30 ± 2.00	9.72/11
	$4.0 < y < 4.5$	14.20 ± 0.50	15.40 ± 0.50	8.86/11	0.84 ± 0.05	16.80 ± 2.00	13.48/11
2(h)	$2.0 < y < 2.5$	18.00 ± 0.50	13.80 ± 0.50	10.77/11	1.20 ± 0.10	12.00 ± 2.00	8.03/11
	$2.5 < y < 3.0$	17.80 ± 0.50	13.90 ± 0.50	5.92/11	1.15 ± 0.10	12.50 ± 2.00	8.62/11
	$3.0 < y < 3.5$	17.60 ± 0.50	14.00 ± 0.50	8.20/11	1.12 ± 0.10	12.80 ± 2.00	10.17/11
	$3.5 < y < 4.0$	16.50 ± 0.50	14.40 ± 0.50	9.56/11	1.05 ± 0.10	14.20 ± 2.00	8.75/11
	$4.0 < y < 4.5$	15.50 ± 0.50	14.60 ± 0.50	13.83/11	1.00 ± 0.05	14.70 ± 2.00	10.58/11

Table A2. Continued. Values of p_0 , n_0 , and χ^2/ndof corresponding to the dashed curves in Figs. 3 and 4, as well as values of T , n , and χ^2/ndof corresponding to the dotted curves in Figs. 3 and 4. The parameter values in the first (second) row in each panel for Fig. 4(d) is for the first (second) component, where * denotes k_H and ** denotes k_L . In other cases only the single component is used.

Figure	Main selection	p_0 (GeV/c)	n_0	χ^2/ndof	T (GeV)	n	χ^2/ndof
3(a)	1.8 TeV	9.00 ± 0.50	12.10 ± 0.50	$4.00/2$	0.65 ± 0.05	9.00 ± 1.00	$5.50/2$
	1.96 TeV	10.30 ± 0.50	12.20 ± 0.50	$17.50/22$	0.75 ± 0.05	9.30 ± 1.00	$9.99/22$
3(b)	Inclusive $\psi(2S)$	14.10 ± 0.50	13.10 ± 0.50	$19.96/2$	1.07 ± 0.10	12.30 ± 2.00	$4.51/2$
	Prompt $\psi(2S)$	14.20 ± 0.50	13.00 ± 0.50	$10.43/2$	1.10 ± 0.10	12.00 ± 1.00	$2.36/2$
	$\psi(2S)$ from b	14.30 ± 0.50	12.80 ± 0.50	$15.75/2$	1.13 ± 0.10	11.70 ± 2.00	$7.59/2$
3(c)	$0.00 < y < 0.75$	14.50 ± 0.50	13.50 ± 0.50	$7.75/2$	1.16 ± 0.10	12.80 ± 1.00	$7.00/2$
	$0.75 < y < 1.50$	14.30 ± 0.50	13.60 ± 0.50	$5.14/2$	1.14 ± 0.10	13.00 ± 1.00	$3.22/2$
	$1.50 < y < 2.00$	14.10 ± 0.50	13.70 ± 0.50	$3.14/2$	1.12 ± 0.10	13.20 ± 1.00	$3.14/2$
	$0.00 < y < 0.75$	16.00 ± 0.50	13.00 ± 0.50	$6.25/2$	1.32 ± 0.10	12.50 ± 1.00	$4.33/2$
3(d)	$0.75 < y < 1.50$	15.90 ± 0.50	13.10 ± 0.50	$9.89/2$	1.31 ± 0.10	12.60 ± 1.00	$7.39/2$
	$1.50 < y < 2.00$	15.80 ± 0.50	13.20 ± 0.50	$11.25/2$	1.30 ± 0.10	12.70 ± 1.00	$10.25/2$
	$0 < y < 0.9$	15.50 ± 0.50	11.20 ± 0.50	$2.00/-$	1.50 ± 0.05	12.00 ± 1.00	$2.21/-$
	$0.9 < y < 1.5$	15.30 ± 0.50	11.30 ± 0.50	$1.85/-$	1.48 ± 0.05	12.20 ± 1.00	$2.69/-$
3(e)	$1.5 < y < 1.93$	15.10 ± 0.50	11.40 ± 0.50	$2.75/-$	1.45 ± 0.05	12.50 ± 1.00	$3.50/-$
	$1.93 < y < 2.4$	14.90 ± 0.50	11.50 ± 0.50	$3.50/-$	1.42 ± 0.05	12.70 ± 1.00	$4.84/-$
	$ y < 1.2$	16.00 ± 0.50	14.50 ± 0.50	$2.39/6$	1.50 ± 0.10	14.50 ± 1.00	$3.39/6$
	$1.2 < y < 1.6$	15.50 ± 0.50	14.80 ± 0.50	$3.80/4$	1.38 ± 0.10	15.00 ± 1.00	$6.67/4$
3(f)	$1.6 < y < 2.4$	15.00 ± 0.50	15.10 ± 0.50	$2.10/4$	1.28 ± 0.10	15.50 ± 1.00	$3.64/4$
	$ y < 1.2$	18.00 ± 0.50	13.00 ± 0.50	$4.17/6$	1.65 ± 0.05	14.00 ± 1.00	$3.98/6$
	$1.2 < y < 1.6$	17.00 ± 0.50	13.50 ± 0.50	$4.23/4$	1.57 ± 0.05	14.50 ± 1.00	$4.86/4$
	$1.6 < y < 2.4$	16.00 ± 0.50	14.00 ± 0.50	$3.49/4$	1.50 ± 0.05	15.00 ± 1.00	$2.89/4$
4(a)	$ y < 0.75$	25.00 ± 0.50	14.00 ± 0.50	$6.84/7$	1.85 ± 0.05	14.00 ± 1.00	$7.88/7$
	$0.75 < y < 1.5$	24.60 ± 0.50	14.20 ± 0.50	$6.81/7$	1.82 ± 0.05	14.30 ± 1.00	$7.69/7$
	$1.5 < y < 2.0$	24.20 ± 0.50	14.40 ± 0.50	$6.64/7$	1.79 ± 0.10	14.60 ± 1.00	$6.67/7$
4(b)	$ y < 0.75$	25.50 ± 0.50	12.50 ± 0.50	$7.78/7$	2.20 ± 0.10	13.00 ± 1.00	$8.77/7$
	$0.75 < y < 1.5$	25.30 ± 0.50	12.60 ± 0.50	$5.70/7$	2.10 ± 0.10	13.20 ± 1.00	$8.45/7$
	$1.5 < y < 2.0$	24.50 ± 0.50	13.00 ± 0.50	$8.56/7$	2.00 ± 0.10	13.40 ± 1.00	$7.03/7$
4(c)	Prompt $\psi(2S)$	26.00 ± 0.50	14.60 ± 0.50	$16.25/2$	1.90 ± 0.05	14.50 ± 1.00	$17.27/2$
	Non-prompt $\psi(2S)$	26.50 ± 0.50	13.00 ± 0.50	$9.40/2$	2.30 ± 0.10	13.50 ± 1.00	$8.59/2$
4(d)	$0.0 < y < 0.3$	35.00 ± 1.00	18.00 ± 1.00	$0.80 \pm 0.05^*$	2.35 ± 0.20	18.00 ± 2.00	$0.75 \pm 0.05^{**}$
		20.00 ± 1.00	9.00 ± 0.50	$3.94/3$	2.35 ± 0.10	8.40 ± 0.50	$4.17/3$
	$0.3 < y < 0.6$	34.50 ± 1.00	18.50 ± 1.00	$0.80 \pm 0.05^*$	2.30 ± 0.20	18.50 ± 2.00	$0.75 \pm 0.05^{**}$
		20.00 ± 1.00	9.00 ± 0.20	$4.08/3$	2.30 ± 0.10	8.20 ± 0.50	$4.47/3$
	$0.6 < y < 0.9$	34.00 ± 1.00	19.00 ± 1.00	$0.80 \pm 0.05^*$	2.25 ± 0.20	19.00 ± 2.00	$0.75 \pm 0.05^{**}$
		20.00 ± 1.00	9.00 ± 0.20	$7.50/3$	2.25 ± 0.10	8.00 ± 0.50	$6.95/3$
	$0.9 < y < 1.2$	33.50 ± 1.00	19.50 ± 1.00	$0.80 \pm 0.05^*$	2.20 ± 0.20	19.50 ± 2.00	$0.75 \pm 0.05^{**}$
		20.00 ± 1.00	9.00 ± 0.20	$9.81/3$	2.20 ± 0.10	7.80 ± 0.30	$6.12/3$

Table A2. Continued. Values of p_0 , n_0 , and χ^2/ndof corresponding to the dashed curves in Figs. 5 and 6, as well as values of T , n , and χ^2/ndof corresponding to the dotted curves in Figs. 5 and 6.

Figure	Main selection	p_0 (GeV/c)	n_0	χ^2/ndof	T (GeV)	n	χ^2/ndof
5(a)	$\Upsilon(1S)$	24.00 ± 1.00	12.50 ± 1.00	56.89/11	1.60 ± 0.10	9.50 ± 2.00	21.67/11
	$\Upsilon(2S)$	26.00 ± 2.00	12.70 ± 1.00	9.75/6	1.75 ± 0.10	9.70 ± 2.00	7.50/6
	$\Upsilon(3S)$	28.00 ± 2.00	12.90 ± 1.00	14.97/6	1.85 ± 0.10	10.50 ± 2.00	7.43/6
5(b)	$\Upsilon(1S)$	27.00 ± 2.00	12.70 ± 1.00	39.17/3	1.65 ± 0.10	11.00 ± 2.00	9.54/3
	$\Upsilon(2S)$	28.00 ± 2.00	12.80 ± 1.00	4.76/3	1.90 ± 0.10	11.50 ± 2.00	4.53/3
	$\Upsilon(3S)$	29.00 ± 2.00	12.90 ± 1.00	2.73/3	2.00 ± 0.10	12.00 ± 2.00	2.90/3
5(c)	$\Upsilon(1S)$	29.00 ± 2.00	12.90 ± 1.00	6.60/3	2.20 ± 0.20	16.00 ± 2.00	5.39/3
	$\Upsilon(2S)$	33.00 ± 2.00	13.00 ± 1.00	6.64/-	2.50 ± 0.20	16.30 ± 2.00	6.69/-
	$\Upsilon(3S)$	34.00 ± 2.00	13.20 ± 1.00	11.25/-	2.60 ± 0.20	16.50 ± 2.00	11.50/-
5(d)	$2.0 < y < 2.5$	31.00 ± 2.00	15.00 ± 1.00	11.65/21	2.30 ± 0.20	19.00 ± 2.00	7.17/21
	$2.5 < y < 3.0$	30.50 ± 2.00	15.50 ± 1.00	9.45/21	2.20 ± 0.20	20.00 ± 2.00	9.48/21
	$3.0 < y < 3.5$	30.00 ± 2.00	16.00 ± 1.00	7.89/21	2.10 ± 0.20	21.00 ± 2.00	6.39/21
	$3.5 < y < 4.0$	29.50 ± 2.00	16.50 ± 1.00	10.06/18	1.95 ± 0.20	23.00 ± 2.00	8.07/18
	$4.0 < y < 4.5$	28.50 ± 2.00	17.50 ± 1.00	9.64/12	1.80 ± 0.20	25.00 ± 2.00	7.98/12
5(e)	$2.0 < y < 2.5$	36.00 ± 2.00	15.20 ± 1.00	15.98/21	2.60 ± 0.20	20.00 ± 2.00	13.23/21
	$2.5 < y < 3.0$	35.50 ± 2.00	15.70 ± 1.00	8.34/21	2.50 ± 0.20	21.00 ± 2.00	10.26/21
	$3.0 < y < 3.5$	35.20 ± 2.00	16.20 ± 1.00	12.84/21	2.40 ± 0.20	22.00 ± 2.00	9.34/21
	$3.5 < y < 4.0$	34.30 ± 1.00	17.00 ± 0.50	10.64/18	2.10 ± 0.20	24.00 ± 2.00	8.31/18
	$4.0 < y < 4.5$	31.00 ± 1.00	17.50 ± 0.50	14.06/12	1.90 ± 0.20	26.00 ± 2.00	11.34/12
5(f)	$2.0 < y < 2.5$	40.00 ± 2.00	15.50 ± 1.00	14.73/21	2.70 ± 0.20	21.00 ± 2.00	15.45/21
	$2.5 < y < 3.0$	39.50 ± 2.00	16.00 ± 1.00	10.85/21	2.60 ± 0.20	22.00 ± 2.00	7.95/21
	$3.0 < y < 3.5$	39.00 ± 2.00	16.50 ± 1.00	12.37/21	2.50 ± 0.20	23.00 ± 2.00	6.78/21
	$3.5 < y < 4.0$	38.50 ± 2.00	17.80 ± 1.00	14.56/18	2.30 ± 0.20	25.00 ± 2.00	8.31/18
	$4.0 < y < 4.5$	37.00 ± 2.00	18.30 ± 1.00	11.37/12	2.10 ± 0.20	26.50 ± 2.00	7.53/12
6(a)	$2.0 < y < 2.5$	32.00 ± 2.00	15.50 ± 1.00	14.23/21	2.35 ± 0.20	22.00 ± 2.00	9.12/21
	$2.5 < y < 3.0$	31.50 ± 2.00	16.00 ± 1.00	7.53/21	2.25 ± 0.20	23.00 ± 2.00	14.76/21
	$3.0 < y < 3.5$	31.00 ± 2.00	16.50 ± 1.00	12.33/21	2.15 ± 0.10	24.00 ± 2.00	7.44/21
	$3.5 < y < 4.0$	30.50 ± 2.00	17.00 ± 1.00	8.72/18	2.05 ± 0.10	25.00 ± 2.00	9.75/18
	$4.0 < y < 4.5$	29.00 ± 2.00	17.50 ± 0.50	13.73/12	1.85 ± 0.10	27.00 ± 2.00	12.03/12
6(b)	$2.0 < y < 2.5$	38.00 ± 2.00	16.00 ± 1.00	16.54/21	2.70 ± 0.20	24.00 ± 2.00	10.98/21
	$2.5 < y < 3.0$	37.50 ± 2.00	16.50 ± 1.00	7.14/21	2.60 ± 0.10	25.00 ± 2.00	12.54/21
	$3.0 < y < 3.5$	37.00 ± 2.00	17.00 ± 1.00	11.25/21	2.50 ± 0.10	26.00 ± 2.00	8.34/21
	$3.5 < y < 4.0$	36.50 ± 2.00	17.20 ± 0.50	10.31/18	2.30 ± 0.10	27.50 ± 2.00	9.51/18
	$4.0 < y < 4.5$	35.00 ± 2.00	17.60 ± 0.50	14.24/12	2.00 ± 0.10	28.50 ± 2.00	5.67/12
6(c)	$2.0 < y < 2.5$	44.00 ± 3.00	16.50 ± 1.00	15.89/21	2.90 ± 0.10	25.00 ± 2.00	9.48/21
	$2.5 < y < 3.0$	43.00 ± 3.00	17.00 ± 1.00	7.53/21	2.80 ± 0.20	25.50 ± 2.00	10.68/21
	$3.0 < y < 3.5$	42.00 ± 3.00	17.50 ± 1.00	13.59/21	2.70 ± 0.10	26.50 ± 2.00	7.53/21
	$3.5 < y < 4.0$	41.00 ± 3.00	18.00 ± 1.00	12.42/18	2.50 ± 0.10	28.00 ± 2.00	7.34/18
	$4.0 < y < 4.5$	38.00 ± 3.00	18.50 ± 1.00	13.59/12	2.23 ± 0.10	29.00 ± 2.00	8.31/12
6(d)	$1.5 < y < 2.0$	34.00 ± 2.00	15.20 ± 1.00	5.35/4	2.45 ± 0.10	22.00 ± 2.00	3.85/4
	$2.0 < y < 2.5$	33.00 ± 2.00	15.70 ± 1.00	4.79/4	2.35 ± 0.10	23.00 ± 2.00	2.20/4
	$2.5 < y < 3.0$	32.50 ± 2.00	16.00 ± 1.00	4.25/4	2.25 ± 0.10	24.00 ± 2.00	2.69/4
	$3.0 < y < 3.5$	32.00 ± 2.00	16.50 ± 1.00	6.72/4	2.15 ± 0.10	25.00 ± 2.00	3.70/4
	$3.5 < y < 4.0$	31.50 ± 2.00	17.00 ± 1.00	7.40/3	2.05 ± 0.10	26.00 ± 2.00	4.40/3
6(e)	$2.0 < y < 2.5$	37.00 ± 3.00	16.00 ± 1.00	16.58/21	2.60 ± 0.10	26.00 ± 2.00	19.66/21
	$2.5 < y < 3.0$	36.00 ± 3.00	16.50 ± 1.00	10.31/22	2.50 ± 0.10	27.00 ± 2.00	14.83/22
	$3.0 < y < 3.5$	35.00 ± 3.00	17.00 ± 0.50	10.28/21	2.40 ± 0.10	28.00 ± 2.00	13.91/21
	$3.5 < y < 4.0$	34.50 ± 3.00	17.50 ± 0.50	13.42/19	2.30 ± 0.10	29.00 ± 2.00	12.85/19
	$4.0 < y < 4.5$	34.30 ± 1.00	17.70 ± 0.50	9.64/13	2.25 ± 0.10	29.50 ± 2.00	8.53/13
6(f)	$2.0 < y < 2.5$	41.00 ± 3.00	16.50 ± 1.00	20.71/21	2.80 ± 0.10	29.00 ± 2.00	12.23/21
	$2.5 < y < 3.0$	40.00 ± 2.00	17.00 ± 0.50	18.20/22	2.70 ± 0.10	30.00 ± 2.00	24.00/22
	$3.0 < y < 3.5$	39.50 ± 2.00	17.20 ± 0.50	7.92/21	2.65 ± 0.10	30.50 ± 2.00	8.31/21
	$3.5 < y < 4.0$	39.20 ± 1.00	17.40 ± 0.50	16.12/19	2.60 ± 0.10	31.00 ± 2.00	14.11/19
	$4.0 < y < 4.5$	39.00 ± 1.00	17.80 ± 0.50	14.17/13	2.50 ± 0.10	32.00 ± 2.00	10.81/13
6(g)	$2.0 < y < 2.5$	47.00 ± 2.00	17.00 ± 1.00	16.98/21	3.20 ± 0.10	30.00 ± 2.00	12.63/21
	$2.5 < y < 3.0$	46.00 ± 2.00	17.50 ± 1.00	19.68/22	3.10 ± 0.10	31.00 ± 2.00	10.16/22
	$3.0 < y < 3.5$	45.50 ± 2.00	17.70 ± 0.50	14.69/21	3.00 ± 0.10	32.00 ± 2.00	10.40/21
	$3.5 < y < 4.0$	45.30 ± 2.00	18.50 ± 1.00	15.60/19	2.90 ± 0.10	33.00 ± 2.00	11.71/19
	$4.0 < y < 4.5$	45.00 ± 2.00	18.80 ± 0.50	14.66/13	2.80 ± 0.10	34.00 ± 2.00	8.86/13

Appendix 2: Figures of parameters and some discussions.

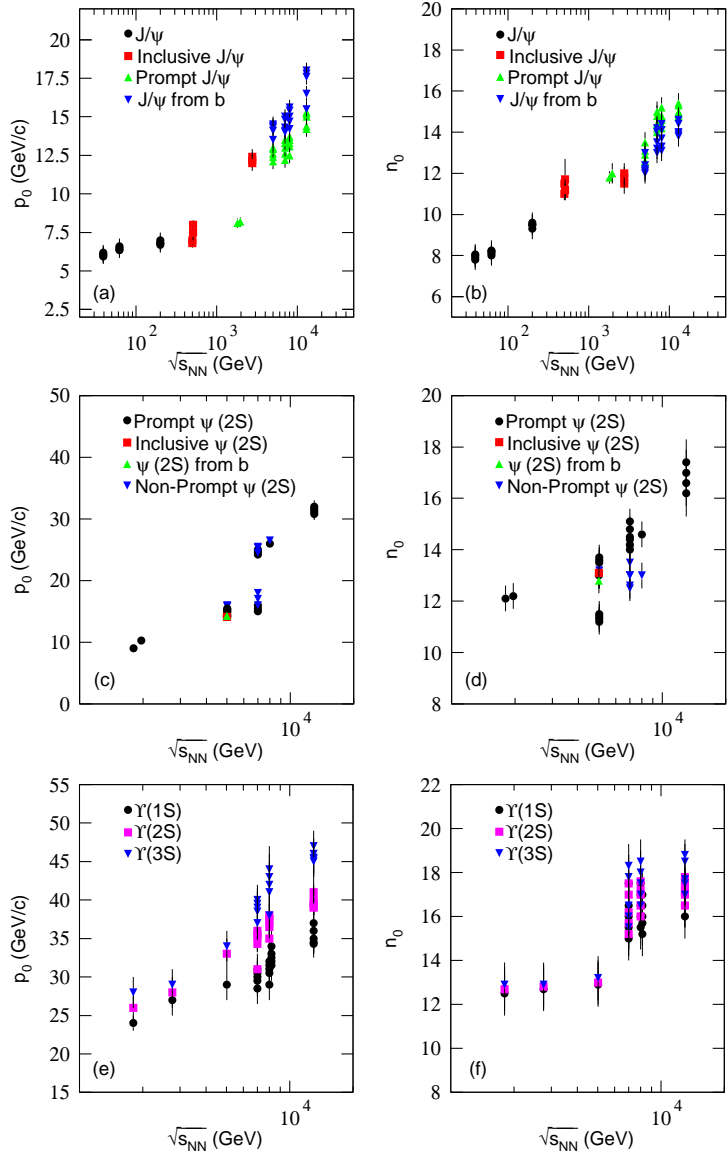


Fig. A1. Same as Fig. 7, but showing the dependences of (a)(c)(e) p_0 and (b)(d)(f) n_0 on $\sqrt{s_{NN}}$ (or \sqrt{s}) for (a)(b) J/ψ , (c)(d) $\psi(2S)$, and (e)(f) $\Upsilon(nS, n = 1, 2, 3)$.

Figure A1 is the same as Fig. 7, but showing the dependences of (a)(c)(e) p_0 and (b)(d)(f) n_0 on $\sqrt{s_{NN}}$ (or \sqrt{s}) for (a)(b) J/ψ , (c)(d) $\psi(2S)$, and (e)(f) $\Upsilon(nS, n = 1, 2, 3)$. The different symbols represent the parameter values derived from free parameters extracted from Figs. 1–6 and listed in Tables A1 and A2. One can see that p_0 and n_0 increases with the increase of collision energy and particle mass.

Figure A2 is the same as Fig. 7, but showing the dependences of (a)(c)(e)(g) p_0 and (b)(d)(f)(h) n_0 on

(a)(b) centrality C and (c)–(h) rapidity y for (a)–(d) J/ψ , (e)(f) $\psi(2S)$, and (g)(h) $\Upsilon(nS, n = 1, 2, 3)$. One can see that p_0 (n_0) increases (decreases) slightly with the increase of event centrality from peripheral to central collisions, and decreases (increase) (slightly) with the increase of rapidity from mid-rapidity to forward rapidity. Meanwhile, p_0 (n_0) increases with the increases of collision energy and particle mass.

Figure A3 is the same as Fig. 7, but showing the dependences of (a)(c)(e) T and (b)(d)(f) n on $\sqrt{s_{NN}}$ (or

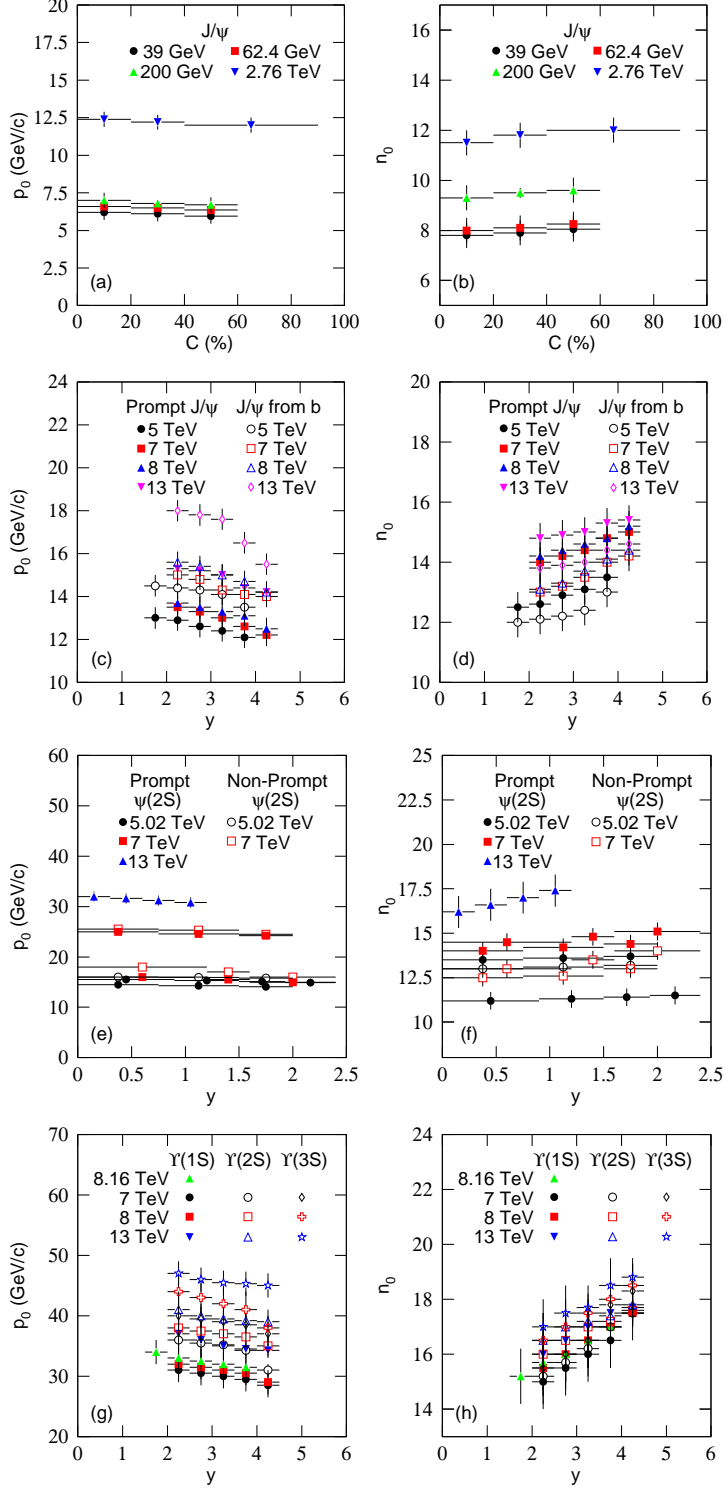


Fig. A2. Same as Fig. 7, but showing the dependences of (a)(c)(e)(g) p_0 and (b)(d)(f)(h) n_0 on (a)(b) C and (c)–(h) y for (a)–(d) J/ψ , (e)(f) $\psi(2S)$, and (g)(h) $\Upsilon(nS, n = 1, 2, 3)$.

\sqrt{s}) for (a)(b) J/ψ , (c)(d) $\psi(2S)$, and (e)(f) $\Upsilon(nS, n = 1, 2, 3)$. One can see that T and n increases with the increase of collision energy and particle mass.

Figure A4 is the same as Fig. 7, but showing the dependences of (a)(c)(e)(g) T and (b)(d)(f)(h) n on (a)(b) centrality C and (c)–(h) rapidity y for (a)–(d)

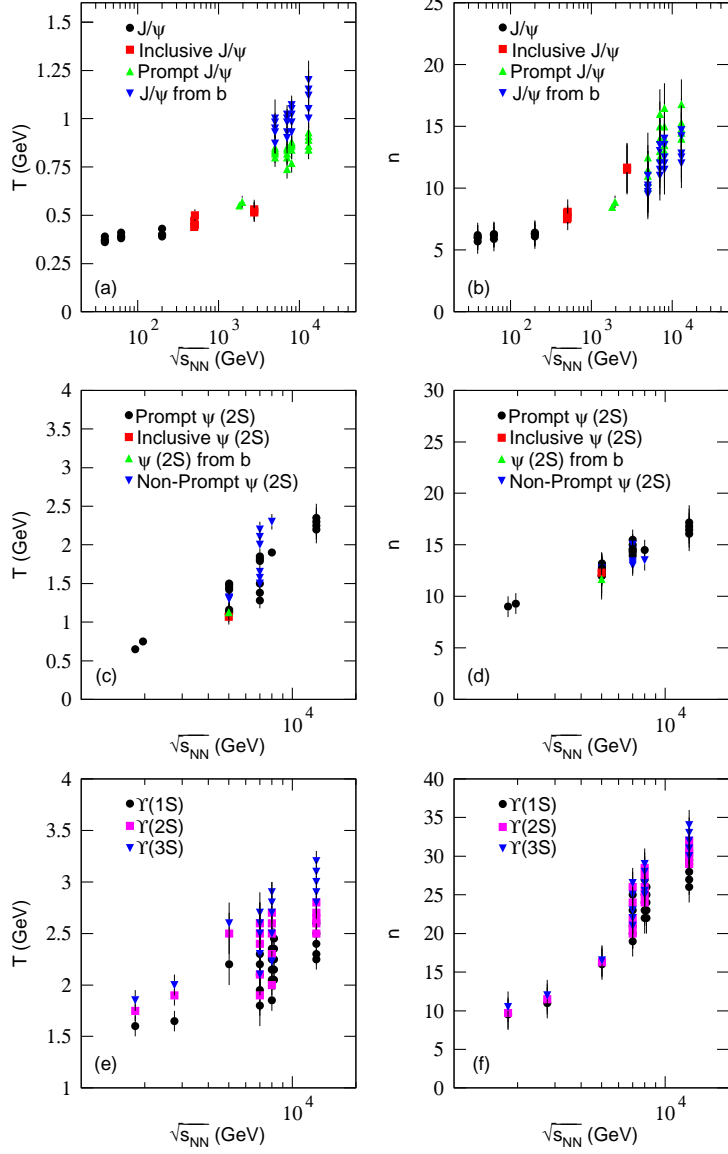


Fig. A3. Same as Fig. 7, but showing the dependences of (a)(c)(e) T and (b)(d)(f) n on $\sqrt{s_{NN}}$ (or \sqrt{s}) for (a)(b) J/ψ , (c)(d) $\psi(2S)$, and (e)(f) $\Upsilon(nS, n = 1, 2, 3)$, where T is not the initial temperature, but an effective temperature parameter in the Tsallis-Levy function.

J/ψ , (e)(f) $\psi(2S)$, and (g)(h) $\Upsilon(nS, n = 1, 2, 3)$. One can see that T (n) increases (decreases) slightly with the increase of event centrality from peripheral to central collisions, and decreases (increase) (slightly) with the increase of rapidity from mid-rapidity to forward rapidity. Meanwhile, T (n) increases with the increases of collision energy and particle mass.

The tendency of $p_0(T)$ and $n_0(n)$ with collision energy are also explained by more violent collision at higher energy. Both $p_0(T)$ and $n_0(n)$ increase with the increase of collision energy. This means that $p_0(T)$ and $n_0(n)$ are positively correlative at different ener-

gies. Meanwhile, for a given p_T spectrum or in given collisions, an increase in $p_0(T)$ is concomitant with a decrease in $n_0(n)$. This means that $p_0(T)$ and $n_0(n)$ are negatively correlative in given collisions (at given energy). There are correlations between $p_0(T)$ and $n_0(n)$ when we determine these parameters.

The correlation between $p_0(T)$ and $n_0(n)$ is similar to that between kinetic freeze-out temperature and transverse flow velocity [60, 61] which also show positive correlation at different energies and negative correlation in given spectrum. If $p_0(T)$ is similar to kinetic freeze-out temperature, $n_0(n)$ should be similar to transverse

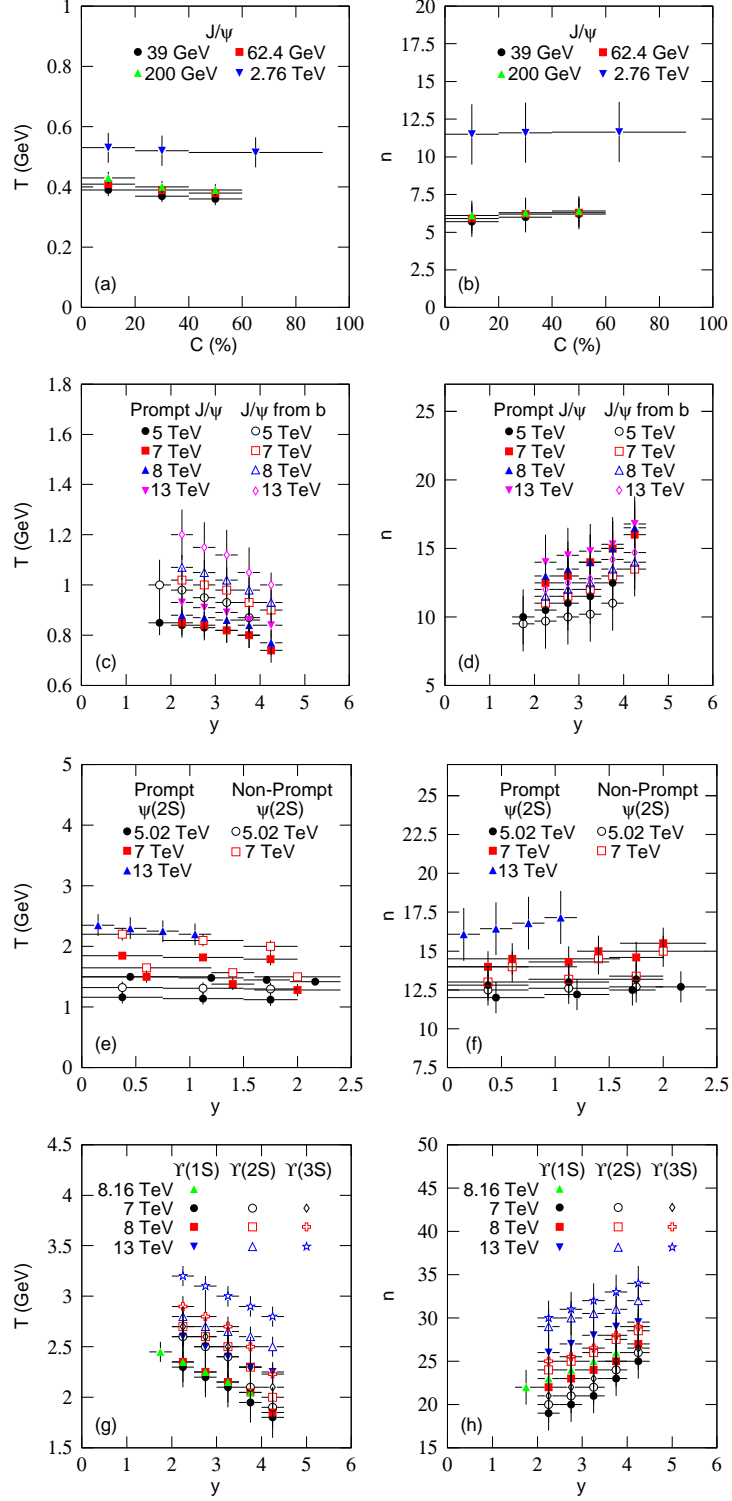


Fig. A4. Same as Fig. 7, but showing the dependences of (a)(c)(e)(g) T and (b)(d)(f)(h) n on (a)(b) C and (c)-(h) y for (a)-(d) J/ψ , (e)(f) $\psi(2S)$, and (g)(h) $\Upsilon(nS, n = 1, 2, 3)$, where T is not the initial temperature, but an effective temperature parameter in the Tsallis-Levy function.

flow velocity. Meanwhile, the results obtained in this work are in agreement with our recent work [62], which shows mass-dependent parameters. In particular, with

the increase of particle mass, $\langle p_T \rangle$, T_i , p_0 , and n_0 increase.